A late Holocene multi-proxy record from the northern Norwegian margin: temperature and salinity variability

Berben SMP[a], Husum K[b] and Aagaard-Sørensen S[a]
[a]Department of Geology, University of Tromsø, N-9037 Tromsø, Norway
[b]Norwegian Polar Institute, Fram Centre, N-9296 Tromsø, Norway

Correspondence to: Berben SMP (sarah.m.berben@uit.no)

Keywords: Atlantic water inflow, Coastal water, NAO, northern Norwegian margin, late Holocene, planktic foraminifera, stable isotopes, Mg/Ca

Abstract

This study presents a late Holocene multi-proxy analysis performed on a marine sediment core from the northern Norwegian margin. Palaeo sub-surface temperature and salinity estimates were reconstructed in order to elucidate the natural variability of Atlantic and Coastal water influences. Planktic foraminiferal fauna and their preservation indicators, stable isotopes ($\delta^{18}O$, $\delta^{13}C$) and trace elements were analysed. Paired Mg/Ca and $\delta^{18}O$ measurements of *N. pachyderma* resulted in temperature ($SST_{Mg/Ca}$) and salinity reconstructions in addition to transfer function derived temperature ($SST_{Transfer}$) estimates. The overall poor preservation conditions at the core site might have influenced the Mg/Ca ratios and are therefore likely the primary cause of the recorded underestimated $SST_{Mg/Ca}$ and SSS values. The high resolution record shows a general cooling trend with fluctuating palaeoceanographic conditions which are attributed to shifting NAO conditions. Period I (ca. 3500 – 2900 cal yr BP) is characterized by a stronger influence of Coastal water and stratified water masses most likely associated with negative NAO-like conditions. During period II (ca. 2900 – 1600 cal yr BP) warm Atlantic water linked with a positive NAO mode dominates the core site. A returned influence of Coastal water is observed throughout period III (ca. 1600 – 950 cal yr BP). The stable and colder sub-surface temperatures during this period correlate with the Dark Ages. Within period IV (ca. 950 – 550 cal yr BP) the core site experienced a stronger influence of Atlantic water likely due to positive NAO conditions correlating to the Medieval Warm Period.

1 Introduction

Throughout the late Holocene, a general cooling trend has been observed in the North Atlantic associated with a reduced influence of warm Atlantic water (e.g. Slubowska et al., 2005; Hald et al., 2007; Skirbekk et al., 2010). A similar cooling trend, recorded by lake and tree records from north-western Europe, has been ascribed to reduced insolation at high latitudes (e.g. Bjune et al., 2009; Kaufman et al., 2009). Contradictory, fluctuations of a strengthened Atlantic water inflow towards the Arctic Ocean have been observed at the Vøring plateau (e.g. Andersson et al., 2003; Risebrobakken et al., 2003; Andersson et al., 2010), the Barents Sea (e.g. Duplessy et al., 2001; Lubinski et al., 2001; Berben et al., 2014)

and the Svalbard margin (e.g. Slubowska-Woldengen et al., 2007; Jernas et al., 2013; Werner et al., 2013; Zamelczyk et al., 2013). Additionally, throughout the late Holocene, several observations of fluctuating climatic conditions have been found in the Nordic Seas (e.g. Giraudeau et al., 2004; Nyland et al., 2006; Solignac et al., 2006; Slubowska-Woldengen et al., 2007) as well as in north-western Europe (e.g. Lauritzen and Lundberg, 1999; Bjune and Birks, 2008). These include the 'Roman Warm Period' (RWP, ca. BCE 50 – CE 400), the 'Dark Ages' (DA, ca. CE 400 - 800), the 'Medieval Warm Period' (MWP, CE 900 – 1500) and the 'Little Ice Age' (LIA, ca. CE 1500 - 1900) (e.g. Lamb, 1977).

These fluctuating conditions have been ascribed to different causes such as solar forcing, volcanic eruptions (e.g. Bryson and Goodman, 1980; Lean, 2002; Jiang et al., 2005; Wanner et al., 2008) or changes in atmospheric forcing linked to the North Atlantic Oscillation (NAO) controlling the inflow of Atlantic water to the Arctic Ocean (e.g. Trouet et al., 2009; Olsen et al., 2012). Warm and salty Atlantic water is brought into the Nordic Seas by the North Atlantic Current (NAC) and flows parallel with colder and less saline Coastal water along the Norwegian margin. These two water masses possess opposite characteristics with respect to temperature and salinity. Further, they respond opposite to the strengthened or reduced westerlies attributed to positive and negative NAO modes, respectively (e.g. Sætre, 2007). A positive versus negative NAO mode affects the climatic conditions in north-western Europe by generating warmer and wetter versus colder and dryer conditions (e.g. Wanner et al., 2001). Along the Norwegian coast the impact of the variable NAO is seen in precipitation, temperature and wind intensity changes (Ottersen et al., 2001). And thus, the northern Norwegian margin is a key location to investigate the natural variability of Atlantic water inflow throughout the late Holocene linked to fluctuating NAO modes. With respect to the recent global warming, it is of great importance to understand the natural variability of the Atlantic water inflow towards the Arctic Ocean as it strongly influences north-western Europe climatic conditions.

For the Nordic Seas, several studies have reconstructed water mass properties based on planktic foraminiferal fauna. Transfer functions reflect sub-surface temperatures whereas stable oxygen isotopes reflect both the temperature and $\delta^{18}O$ of ambient sea water (e.g. Sarnthein et al., 2003; Rasmussen and Thomsen, 2010; Risebrobakken et al., 2010; Berben et al., 2014). However, in order to reconstruct palaeo sub-surface salinities, additional proxies are required. The Mg-uptake in foraminiferal calcite is primarily temperature depended (e.g.

Nürnberg, 1995). The positive correlation between the Mg-uptake in foraminiferal calcite and temperature of the ambient sea water during growth allows palaeo reconstructions of sub-surface temperatures based on Mg/Ca ratio measurements (e.g. Mashiotta et al., 1999; Elderfield and Ganssen, 2000; Kozdon et al., 2009). Therefore, paired calcite $\delta^{18}O$ and Mg/Ca measurements enable the reconstruction of palaeo seawater $\delta^{18}O$ (e.g. Thornalley et al., 2009; Elderfield et al., 2010) and subsequently, via modern $\delta^{18}O_{seawater}$:salinity relationships, enable the reconstruction of palaeo salinity.

In order to investigate the fluctuating interplay of Atlantic and Coastal water related to variable NAO modes throughout the late Holocene, the variability of sub-surface temperature and salinity has been reconstructed. Paired Mg/Ca and $\delta^{18}O$ measurements of *Neogloboquadrina pachyderma* were analysed in addition to the distribution of planktic foraminiferal fauna and preservation conditions. Subsequently, a new record of both palaeo sub-surface temperature and salinity estimates from the northern Norwegian margin is presented.

2 Present day oceanography

The Norwegian Sea is dominated by relatively warm and saline Atlantic water (>2 °C, >35 ‰; Hopkins, 1991). Atlantic water is brought to the area by the two-branched Norwegian Atlantic Current (NwAC) (Orvik and Niiler, 2002) (Figure 1A). Both branches follow a topographically steered northwards pathway through the Nordic Seas and eventually reach the Arctic Ocean via the Fram Strait. The western branch crosses the Iceland-Faroe Ridge entering the Norwegian Sea as the Iceland-Faroe frontal jet (Perkins et al., 1998) (Figure 1A). The eastern branch passes through the Faroe-Shetland channel and follows a pathway along the Norwegian shelf edge towards the Arctic Ocean with a branch flowing into the Barents Sea (Orvik and Niiler, 2002) (Figure 1A).

The Norwegian Coastal Current (NCC) transports Coastal water (2-13 °C, 32-35 ‰; Hopkins, 1991) northwards originating from the North Sea, the Baltic and the Norwegian coast (Figure 1A). Coastal water is characterized by its low salinities due to the influence of freshwater run off from the Norwegian mainland. The NCC is density driven which is mainly influenced by its salinity distribution. Mixing with Atlantic water takes place and increases northwards, and

thus salinity increases whereas stratification reduces. In general, cold Coastal water can be found above warmer Atlantic water in the upper 50 to 100 m of the water column as a thinning wedge westwards (Ikeda et al., 1989) (Figure 1B). A boundary is formed as a well-defined front between the cold, low salinity Coastal water and the warmer, more saline Atlantic water (Ikeda et al., 1989). The overall properties and movements of the NCC are influenced by several factors such as freshwater, tides, wind conditions, bottom topography and Atlantic water (Sætre, 2007). In the study area, the topography causes the NCC to extend much further westwards and hence, closer to the influence of the NwAC (Figure 1C). Therefore, this is a key area to investigate the interplay between Atlantic and Coastal water fluctuations as a result of climatic variability.

3 Material and methods

For this study, a marine sediment core from the northern Norwegian margin (Vøring plateau in front of Trænadjupet south of the Lofoten) was investigated. The core (W00-SC3) (67.24° N, 08.31° E) was retrieved in 2000 by the SV *Geobay* at a water depth of 1184 m (Laberg et al., 2002) (Figure 1). Its recovery was 385 cm from which the top 19 cm was disturbed and therefore not used. The core consists of very soft clay sediments and was sampled for each 1.0 cm between 19 and 263 cm. CTD data nearby the core site (67.10° N, 08.26° E) indicate the presence of Atlantic water till a water depth of ca. 375 m for present day conditions (Blaume, 2002) (Figure 2).

3.1 Chronology

A depth-age model of W00-SC3 based on four AMS ^{14}C dates measured on *N. pachyderma* was developed. All four AMS ^{14}C dates were calibrated using Calib 7.0.0 software (Stuiver and Reimer, 1993), the Marine13 calibration curve (Reimer et al., 2013) and a local reservoir age (ΔR value) of 71 ± 21 following recommendations by Mangerud et al. (2006) (Table 1). The calibration was constrained on a 2-σ range for both calendar years Before Present (cal yr BP) and calendar years Before Common Era (BCE)/Common Era (CE) (cal yr BCE/CE). For this study the cal yr BP depth-age model will be used, however, the cal yr BCE/CE scale was

added for all the plotted data in order to compare with different studies. The AMS ^{14}C date at 23.5 cm was omitted from the final depth-age model as it appeared too old. The new depth-age model was constrained using linear interpolation between dated levels. Further, based on the homogeneous lithology throughout the core, the sedimentation rate from 120-40 cm was extrapolated towards the top, more specifically between 40 and 19 cm (Figure 3). The resulting depth-age model is constrained between 3485 and 550 cal yr BP (1536 BCE – 1395 CE) and showed sedimentation rates between 0.79 and 0.87 mm/yr and thus, enabled the sampling on a multi-decadal temporal resolution (Figure 3).

3.2 Planktic foraminifera and preservation indicators

All samples were freeze-dried, wet-sieved through three different size fractions (1000, 100 and 63 µm) and subsequently dried in an oven at 40 °C. Every 4 cm from the 100 - 1000 µm size fraction was analysed for its planktic foraminiferal content (>300 specimens) following Knudsen (1998). The identification of left and right coiling *N. pachyderma* was done following Darling et al. (2006), meaning that the right coiling form is identified as *Neogloboquadrina incompta* (Cifelli, 1961). Subsequently, relative abundances (%) of each species were calculated for 62 samples. The planktic foraminiferal concentration (#/g sediment) and fluxes (#/cm^2/yr) were calculated. For the latter, a theoretical value for the dry bulk density of 0.76 g/cm^3 was assumed based on marine sediment core T-88-2 (Aspeli, 1994) and subsequently calculated according Ehrmann and Thiede (1985).

As carbonate dissolution might affect the planktic foraminiferal assemblages, it is important to investigate the preservation conditions in order to assess the potential dissolution induced pre- and post-depositional alterations (e.g. Zamelczyk et al., 2013). Preservation indicators such as the mean shell weight (µg) of *N. pachyderma* (Broecker and Clark, 2001; Barker and Elderfield, 2002; Beer et al., 2010) and fragmentation (%) of planktic foraminiferal tests (Conan et al., 2002) were inspected. The mean shell weight of *N. pachyderma* was determined for 118 samples using a Mettler Toledo microbalance (0.1 µg sensitivity). In order to minimize problems of variations due to size difference and ontogeny, 50 square shaped and well preserved (visually) specimens were selected from a narrow size range (150 - 250 µm) (Barker et al., 2004). For 62 samples within the 100 - 1000 µm size fraction, the fragmentation was calculated using the equation of Pufhl and Shackleton (2004) (Equation 1).

$$Fragmentation\ (\%) = \frac{\#\ fragments/g}{\#fragments/g/2 + \#\ tests/g} * 100 \qquad \text{[Equation 1]}$$

Within this equation, a divisor (2) is included as it is most likely that each test breaks into more than one fragment. The latter is in order to reduce possible misinterpretations of the dissolution sensitivity in changes and progress (Le and Shackleton, 1992; Pufhl and Shackleton, 2004).

3.3 Geochemical analysis

Weight percentages (wt. %) of total carbon (TC) and total organic carbon (TOC) were analysed at one cm resolution using a LECO SC-444 (ES-2) at the Laboratory of the Geological Survey of Norway (NGU). Prior to TOC analysis, the inorganic carbon (carbonate) was removed by treating the samples with 10 % hydrochloric acid (HCl). The calcium carbonate ($CaCO_3$) content was calculated according Espitalié et al. (1977) (Equation 2).

$$CaCO_3 = (TC - TOC) * 8{,}33 \qquad \text{[Equation 2]}$$

3.4 Stable isotope analysis

Stable isotope analysis ($\delta^{18}O$, $\delta^{13}C$) was performed on 117 samples containing 50 specimens of *N. pachyderma*. In order to minimize size dependent effects on isotopic composition, all specimens were picked in a 150 - 250 µm size fraction (Keigwin and Boyle, 1989; Oppo and Fairbanks, 1989; Donner and Wefer, 1994; Aksu and Vilks, 1998; Bauch et al., 2000). The stable isotope measurements were performed with a Finnigan MAT 253 Mass Spectrometer coupled to an automated Kiel device at the Geological Mass Spectrometer (GMS) Laboratory of the University of Bergen. The analytical errors for $\delta^{18}O$ and $\delta^{13}C$ were ± 0.06 ‰ and ± 0.03 ‰ respectively. The data were reported in ‰ versus VPDB and calibrated with NBS-19. For $\delta^{18}O$, a vital effect of 0.6 ‰ has been applied. This value has previously been suggested for the Nordic Seas (Simstich et al., 2003) as well as for the Norwegian Sea (Nyland et al., 2006).

3.5 Trace element analysis

Trace element analysis was performed on 101 samples containing an average of 75 visually well preserved specimens of the planktic foraminifer *N. pachyderma.* In order to minimize the possible size-dependent bias on the Mg/Ca measurements, the tests were picked from a narrow (as narrow as possible) size fraction (150 - 250 µm) (Elderfield et al., 2002). The tests were cracked open between glass plates in order to optimize the chemical cleaning procedure which consisted of a reduction step to remove metal oxides and an oxidation step to remove any organic matter (e.g. Boyle and Keigwin, 1985). Subsequently, the samples were analysed by ICP-MS method for foraminiferal analysis including simultaneous measurements of Mg, Mn, Al, and Fe, all of which are reported as ratios to Ca. The measurements were performed on a Finnigan Element2 at the Marine Science Institute, UC Santa Barbara with an analytical precision of 1.2 % for Mg/Ca. Fe, Al and Mn are tracers of contaminating phases and thus investigated in order to identify remnant post cleaning sample contamination which might bias the measured Mg/Ca ratios in foraminiferal calcite (Barker et al., 2003).

3.6 Temperature and salinity reconstructions

To reconstruct summer sub-surface temperatures ($SST_{Transfer}$) (July-August-September) for a water depth of 100 m, a transfer function and the modern training set of Husum and Hald (2012) were used. Although the core site lays at the geographical southern boundary of this modern training set, it was assumed to be the most appropriated as it uses material analysed at the >100 µm size fraction and thus include smaller specimens as *Turborotalita quinqueloba* and *Globigerinita uvula*. The transfer function derived $SST_{Transfer}$ reconstructions were performed using C2 version 1.7.2. (Juggins, 2010) and a three component Weighted Average-Partial Least Square (WA-PLS) statistical model with a leave-one-out cross validation (Ter Braak and Juggins, 1993; Telford and Birks, 2005).

Mg/Ca derived sub-surface temperature estimates ($SST_{Mg/Ca}$) were reconstructed using the refined species-specific temperature:Mg/Ca equation of Kozdon et al. (2009) (Equation 3).

$$Mg/Ca\,(mmol/mol) = 0.13\ (\pm 0.037) * T\ (°C) + 0.35\ (\pm 0.17) \qquad \text{[Equation 3]}$$

This equation is based on cross-calibrated $\delta^{44/40}$Ca and Mg/Ca temperature estimates from Holocene core top samples of *N. pachyderma* from the Norwegian Sea and Arctic domain. Although the Mg-uptake into foraminiferal calcite is controlled by exponential thermodynamics (Mashiotta et al., 1999), in Equation 3, it is assumed that within the narrow temperature range occupied by *N. pachyderma*, a linear temperature function is appropriate and works well for reconstructed temperatures above ca. 2.5 °C (Kozdon et al., 2009). However, for temperatures below 2.5 °C, associated with salinities less than 34.5 ‰, the method loses its precision (Kozdon et al., 2009).

In order to reconstruct sub-surface salinities, the oxygen isotope ratios of the ambient seawater ($\delta^{18}O_w$) were first calculated using the temperature:δ^{18}O equation of Shackleton (1974) modified after O'Neil et al. (1969) (Equation 4).

$$T\ (°C) = 16.90 - 4.38 * (\delta^{18}O_c - \delta^{18}O_w) + 0.10 * (\delta^{18}O_c - \delta^{18}O_w)^2 \quad \text{[Equation 4]}$$

Within this equation, T refers to the previously calculated $SST_{Mg/Ca}$, $\delta^{18}O_c$ to the measured oxygen isotope value of foraminiferal calcite (*N. pachyderma*) and $\delta^{18}O_w$ to the oxygen isotope composition of ambient seawater. Both $\delta^{18}O_c$ and $\delta^{18}O_w$ are expressed as ‰ VPDB. In order to convert $\delta^{18}O_w$ VPDB values to the $\delta^{18}O_w$ VSMOW scale, the following equation was applied (Hut, 1987) (Equation 5).

$$\delta^{18}O_{w\,VPDB} = \delta^{18}O_{w\,VSMOW} - 0.27\ ‰ \quad \text{[Equation 5]}$$

Subsequently, Equation 4 and 5 are rearranged in order to calculate $\delta^{18}O_w$ VSMOW which results in Equation 6 (Nyland et al., 2006).

$$\delta^{18}O_w = \delta^{18}O_c + 0.27 - \left[\frac{4.38 - \sqrt{4.38^2 - 0.4 * (16.9 - T_{Mg/Ca})}}{0.2}\right] \quad \text{[Equation 6]}$$

Subsequently, sub-surface salinities (SSS) were reconstructed using the salinity (S) to $\delta^{18}O_w$ relation for the central and eastern Nordic Seas by Simstich et al. (2003) (Equation 7).

$$\delta^{18}O_w = -12.17 + 0.36 * S \quad \text{[Equation 7]}$$

4 Results

4.1 Planktic foraminifera and preservation indicators

The planktic foraminiferal fauna consist of six species: *N. pachyderma*, *T. quinqueloba*, *N. incompta*, *Globigerinita glutinata*, *Globigerina bulloides* and *Globigerinita uvula* (Table 2) (Figure 4). Overall, the record is dominated by *N. incompta* and *T. quinqueloba* with a mean value of ca. 34 and 29 % respectively.

Between ca. 3500 and 2900 cal yr BP, the planktic foraminiferal concentration and flux show relative low values of ca. 750 #/g sediment and ca. 50 #/cm^2/yr (Figure 4A; 5E). *N. pachyderma* and *N. incompta* show a small decrease from ca. 18 to 14 % and from ca. 40 to 22 % (Figure 4B; 4D). Simultaneously, *T. quinqueloba* and *G. uvula* show a gradual increase from ca. 28 to 35 % and from ca. 5 to 20 % (Figure 4C; 4G). *G. glutinata* and *G. bulloides* show relative abundances of ca. 6 and 3 % (Figure 4E; 4F).

The planktic foraminiferal concentration and flux show slightly higher values of ca. 1000 #/g sediment and ca. 65 #/cm^2/yr between ca. 2900 and 2300 cal yr BP which are followed by a sharp increase reaching the highest recorded values (3765 #/g sediment, 226 #/cm^2/yr) towards ca. 1600 cal yr BP (Figure 4A; 5E). Between ca. 2900 and 1600 cal yr BP, stable abundances of *N. pachyderma* (ca. 11 %) and relative high and stable values of *N. incompta* (ca. 33 %) are recorded (Figure 4B; 4D). *T. quinqueloba* shows high values (ca. 32 %) with a gentle decrease towards ca. 1600 cal yr BP (Figure 4C). *G. glutinata* and *G. bulloides* show, in particular between ca. 2900 and 2300 cal yr BP, the highest recorded values (ca. 7 and 5 %) followed by a small reduction between 2300 and 1600 cal yr BP (Figure 4E; 4F).

At ca. 1600 cal yr BP, the concentration and flux records show a rapid drop from 3765 to 865 # g/sediment and from 226 to 52 #/cm^2/yr followed by stable values (ca. 1330 #/g sediment, ca. 80 #/cm^2/yr) between ca. 1600 and 950 cal yr BP (Figure 4A; 5E). Gently increasing values of *G. uvula* (ca. 15 to 26 %) and *G. glutinata* (ca. 2 to 5 %) are recorded; whereas *T. quinqueloba* shows a slight decrease from ca. 25 to 16 % (Figure 4G; 4E; 4C). *N. pachyderma*, *N. incompta* and *G. bulloides* remain relatively constant throughout this period (Figure 4B; 4D; 4F).

Between ca. 950 and 550 cal yr BP, the concentration and flux record show slightly decreasing values towards 450 #/g sediment and 27 #/cm^2/yr (Figure 4A; 5E). *N. pachyderma* and *N. incompta* both show an increase with values up to ca. 23 and 42 % (Figure 4B; 4D). Simultaneously, decreasing values are recorded for *G. glutinata* from ca. 5 to 2 % and for *G. uvula* from ca. 26 to 8 % (Figure 4E; 4G). *T. quinqueloba* and *G. bulloides* remain constant around values of ca. 21 and 2 % respectively (Figure 4C; 4F).

The preservation indicators show overall values between 47 and 94 % of planktic foraminiferal fragmentation and between 1.6 and 4.8 µg for the mean shell weight of *N. pachyderma* (Figure 5A-B). Between ca. 3500 and 2900 cal yr BP, the fragmentation shows generally high values around ca. 75 %, whereas the mean shell weight decreases slightly from 3.7 to 2.6 µg. Between ca. 2900 and 1600 cal yr BP, the fragmentation remains relatively stable around slightly reduced values of ca. 69 %. The mean shell weight of *N. pachyderma* shows decreasing values towards 1.7 µg at ca. 2300 cal yr BP followed by an increase reaching ca. 3 µg at ca. 1600 cal yr BP. Between ca. 1600 and 950 cal yr BP, the fragmentation increases from 49 to 79 % and the mean shell weight remains stable around ca. 2.7 µg. Between ca. 950 and 550 cal yr BP, both preservation indicators show a pronounced increase from ca. 47 to 90 % for the planktic foraminiferal fragmentation and from 2.0 to 3.2 µg for the mean shell weight of *N. pachyderma*.

4.2 Geochemical analysis

The TOC and $CaCO_3$ results show an overall increasing trend with values between 0.7 and 1.3 wt. % and 17.0 and 30.6 wt. %, respectively (Figure 5C-D). Between ca. 3500 and 2900 cal yr BP, both records show an increase of ca. 0.7 to 0.9 wt. % for TOC and ca. 17 to 22 wt. % for $CaCO_3$. Towards ca. 2300 cal yr BP, TOC values increase reaching 1.1 wt. % followed by a quick drop to 0.8 wt. % around ca. 2200 cal yr BP and remain further stable around this value towards ca. 1600 cal yr BP. Between ca. 2900 and 1600 cal yr BP, the $CaCO_3$ continues its increasing trend from ca. 22 to 30 wt. %. Between ca. 1600 and 950 cal yr BP, the TOC values increase gradually from 1.0 to 1.1 wt. %, whereas the $CaCO_3$ data decreases from ca. 30 to 24 wt. %. Between ca. 950 and 550 cal yr BP, TOC values remain relatively stable around ca. 1.0 wt. %, whereas the $CaCO_3$ record increases slightly towards ca. 26 wt. %.

4.3 Stable isotope analysis

The stable isotope analysis results in values between 2.3 and 3.1 ‰ for $\delta^{18}O$ and within the range -0.4 to 0.6 ‰ for $\delta^{13}C$ (Figure 6). Between ca. 3500 and 2900 cal yr BP, $\delta^{18}O$ values decrease gently from ca. 2.9 to 2.7 ‰ whereas the $\delta^{13}C$ record shows simultaneously increasing values from ca. 0.2 to 0.4 ‰. Between ca. 2900 and 1600 cal yr BP, the $\delta^{18}O$ record continues its decreasing trend towards values of 2.5 ‰ at ca. 1600 cal yr BP. The $\delta^{13}C$ values decrease from ca. 0.4 ‰ at ca. 2900 cal yr BP towards ca. 0.1 ‰ at ca. 2300 cal yr BP followed by relative stable values around ca. 0.3 ‰ towards ca. 1600 cal yr BP. Between ca. 1600 and 950 cal yr BP, $\delta^{18}O$ values initially continue their decreasing trend towards 2.4 ‰ at ca. 1300 cal yr BP before increasing to values of ca. 2.7 ‰ between ca. 1200 and 950 cal yr BP. The $\delta^{13}C$ record shows increasing values from ca. 0.1 to 0.4 ‰ during this time interval. Between ca. 950 and 550 cal yr BP both records increase simultaneously towards ca. 2.8 ‰ for $\delta^{18}O$ and ca. 0.5 ‰ for $\delta^{13}C$.

4.4 Trace element analysis

Tracers of contamination are plotted against Mg/Ca ratios (Figure 7). Fe and Al are tracers of detrital material contamination such as silicate minerals, whereas Mn is a tracer of secondary diagenetic Mn-rich carbonate (Boyle, 1983). The results show high correlations between Mg/Ca and Fe and Al tracers, with $R^2 = 0.57$ for Fe/Ca and $R^2 = 0.47$ for Al/Ca (Figure 7A-B). The correlation between Mg/Ca and Mn/Ca is low ($R^2 = 0.06$) and thus further not relevant (Figure 7C). When deleting samples with ratios higher than 100 µmol/mol of the contamination tracers following the contamination threshold used by Barker et al. (2003), the correlations are strongly reduced to non-existing with $R^2 = 0.05$ for Fe/Ca and $R^2 = 0.09$ for Al/Ca (Figure 7D-E). This change suggests that contamination by detrital material (i.e. high values of Fe/Ca and/or Al/Ca) impact the results by elevating the Mg/Ca values. Therefore, all samples (n=32) with ratios >100 µmol/mol of Fe and Al are omitted from the further study.

The resulting Mg/Ca record consists of 69 data points with ratios in the range 0.70 to 0.96 mmol/mol (Figure 8A). Between ca. 3500 and 2900 cal yr BP, the Mg/Ca record shows relative stable values around ca. 0.76 mmol/mol. Between ca. 2900 and 2500 cal yr BP, the ratios increase towards 0.89 mmol/mol. Due to the omitted data as a result of possible

contamination, there is no reliable data between ca. 2500 and 2100 cal yr BP. Between ca. 2100 and 1600 cal yr BP, the record remains relatively stable around ca. 0.81 mmol/mol. Around ca. 1600 cal yr BP the Mg/Ca ratios drop quickly towards 0.70 mmol/mol, thereafter they remain stable around ca. 0.78 mmol/mol towards the top of the record (i.e. due to the omitted values after ca. 800 cal yr BP).

4.5 Temperature and salinity reconstructions

The transfer function derived temperature ($SST_{Transfer}$) reconstructions (n=62) range between 6.3 and 7.7 °C (Figure 8C; 4H). Between ca. 3500 and 2900 cal yr BP, the $SST_{Transfer}$ record decreases from 7.2 to 6.7 °C. Thereafter, the $SST_{Transfer}$ values increase towards ca. 7.7 °C at ca. 2500 cal yr BP. Hereafter the $SST_{Transfer}$ record decreases towards ca. 1600 cal yr BP reaching ca. 6.6 °C. Between ca. 1600 and 950 cal yr BP, the $SST_{Transfer}$ estimates remain relatively stable around ca. 6.6 °C. Eventually, between ca. 950 and 550 cal yr BP, the $SST_{Transfer}$ record shows a decrease of ca. 0.5 °C (from ca. 6.8 to 6.3 °C).

The Mg/Ca derived sub-surface temperature reconstructions ($SST_{Mg/Ca}$) (n=69) range between 2.7 and 4.7 °C (Figure 8B). Between ca. 3500 and 3300 cal yr BP, the $SST_{Mg/Ca}$ values show a small decrease from 3.1 to 2.7 °C followed by relatively stable values of ca. 3.2 °C towards ca. 2900 cal yr BP. Between ca. 2900 and 2500 cal yr BP, the $SST_{Mg/Ca}$ values show a gradual increase from ca. 3.2 to 4.2 °C and between ca. 2100 and 1600 cal yr BP, $SST_{Mg/Ca}$ values are relatively stable around 3.5 °C. Between ca. 1600 and 950 cal yr BP, the $SST_{Mg/Ca}$ estimates are slightly lower around ca. 3.2 °C with one exception around ca. 1300 cal yr BP where $SST_{Mg/Ca}$ estimates peak to 4.7 °C.

Reconstructed sub-surface salinities (SSS) (n=65) range between 31.6 and 34.0 ‰ (Figure 8D). Between ca. 3500 and 2900 cal yr BP, the reconstructed SSS estimates show a gradual decrease from ca. 33 to 32 ‰. After ca. 2900 cal yr BP, the SSS data increases to 33.6 ‰ at ca. 2800 cal yr BP followed by a decrease to ca. 2500 cal yr BP. Between ca. 2100 and 1600 cal yr BP, palaeo SSS estimates are stable around ca. 33 ‰, showing the highest values of the record (i.e. 34.0 ‰). Between ca. 1600 and 950 cal yr BP, the SSS values show stable values of ca. 32 ‰.

5 Discussions

5.1 Palaeo SST and SSS assessment

Modern sea temperature measured nearby the core site is ca. 7 °C within the upper 300 m of the water column (Blaume, 2002) (Figure 2), and thus corresponds to the reconstructed palaeo $SST_{Transfer}$ estimates (Figure 4H; 8C). However, the $SST_{Mg/Ca}$ estimates, which range 3.0 to 3.6 °C lower than the $SST_{Transfer}$, do not correspond with the modern sea temperature data (Figure 8B). Further, the SSS estimates (ca. 33 ‰) show (consequently) lower values than the modern salinity values (>35 ‰) (Blaume, 2002) (Figure 2). Furthermore, the $SST_{Mg/Ca}$ estimates also seem to be rather low compared to palaeo reconstructions of the last 1200 years from the Vøring plateau (Nyland et al., 2006). This dissimilarity is in the first place attributed to the use of a different temperature:Mg/Ca equation by Nyland et al. (2006), more specifically the equation from Elderfield and Ganssen (2000). The temperature:Mg/Ca equations from Elderfield and Ganssen (2000) and Kozdon et al. (2009) are calibrated differently resulting in two different potential temperature ranges of the equations, 0 to 7 °C and 3 to 6 °C respectively. In this study, applying the temperature:Mg/Ca equation of Elderfield and Ganssen (2000) would have resulted in 0.7 to 1.8 °C warmer $SST_{Mg/Ca}$ and 0.71 to 0.88 ‰ higher SSS estimates. Nonetheless, a different equation would still have resulted in lower $SST_{Mg/Ca}$ estimates in comparison with the $SST_{Transfer}$ and/or present day instrumental data. This discrepancy might be caused by variability of the species-specific habitat depth preference and/or main calcification period (i.e. season) of *N. pachyderma*, in addition to initial low Mg/Ca values (Meland et al., 2006; Kozdon et al., 2009).

Whereas the $SST_{Transfer}$ record is reconstructed for a water depth of 100 m, the $SST_{Mg/Ca}$ record reflects the average calcification depth of *N. pachyderma*. Studies have shown a poor correlation between modern Mg/Ca inferred temperatures and their corresponding hydrographic data and thus, contest the previously made assumption that the $SST_{Mg/Ca}$ reflects a constant average calcification depth (Meland et al., 2006; Nyland et al., 2006). The water depth of chamber formation and encrustation of *N. pachyderma* is linked to the stratification of the water column and can therefore be highly variable (e.g. Kohfeld et al., 1996; Stangeew, 2001; Simstich et al., 2003). Furthermore, Kozdon et al. (2009) argued that the main factor controlling the habitat depth of *N. pachyderma* in the Nordic Seas is the density-driven water mass stratification. Therefore, it seems that the by Mg/Ca recorded temperature signal is

bound to the isopycnal layer and hence, only reflects a narrow temperature range. Hemleben et al. (1989) indicated that *N. pachyderma* is probably a passive dweller implying that the water mass stratification is preconditioning the habitat and thus, causing a lower temperature response of the Mg/Ca signal. This effect might even be amplified in high latitudes due to the stronger water mass stratification. It is thus most likely that *N. pachyderma* does not possess a constant calcification depth and that the species therefore records a dampened amplitude of the total sub-surface water temperature range. Due to the distinctive seasonality and strong stratification in high latitude regions, the assignment of a true calcification depth and hence temperature remains one of the major issues (Barker et al., 2003). The apparent calcification depth of *N. pachyderma* can be found around ca. 250 m water depth off Norway (Simstich et al., 2003). Palaeo water mass properties at ca. 250 m might have differed from those at ca. 100 m and thereby possibly partly contributed to the observed discrepancy between $SST_{Mg/Ca}$ and $SST_{Transfer}$ estimates.

On an annual time scale, the biological production of *N. pachyderma* peaks in spring and a second time during maximum stratification in late summer (Jonkers et al., 2010). Therefore, the Mg-uptake by *N. pachyderma* reflects a combined spring and summer temperature signal resulting in lower $SST_{Mg/Ca}$ estimates compared to the $SST_{Transfer}$ values which are reconstructed for summer. However, Jonkers et al. (2013) measured Mg/Ca values of *N. pachyderma* from sediment traps in the central Irminger Sea which only show a weak seasonal trend. Jonkers et al. (2013) speculate that the Mg-uptake is controlled by other factors than temperature such as sensitivity of *N. pachyderma* to $[CO_3^{2-}]$ changes which could partly mask the summertime increases due to a parallel increase in $[CO_3^{2-}]$.

In addition to temperature, several secondary factors might influence the absolute Mg/Ca ratios including variability in salinity (Nürnberg et al., 1996; Lea et al., 1999), calcite dissolution (Dekens et al., 2002), test size (e.g. Elderfield et al., 2002) and the applied cleaning protocol (e.g. Barker et al., 2003), which may provide an explanation to the initially low Mg/Ca values. The presented Mg/Ca ratios are relatively low and are ca. 0.16 mmol/mol lower than previous observations from the Vøring plateau performed within a comparable size fraction using a similar cleaning method (Nyland et al., 2006). In particular, the "Cd cleaning method" (Boyle and Keigwin, 1985) comprising a reductive cleaning step could result in absolute lowering of Mg/Ca ratios of up to ~15 % (Barker et al., 2003; Meland et al., 2006). Artificially correcting the present Mg/Ca data for this potential reduction would translate into

0.8 to 1.1 °C higher $SST_{Mg/Ca}$ and 0.6 to 0.8 ‰ higher SSS estimates, which are still lower than modern day values and the $SST_{Transfer}$ record. Hence, this cleaning step does not seem to explain the differences observed between the two temperature proxies. This was also concluded by Aagaard-Sørensen et al. (2013) after comparisons between transfer function and Mg/Ca derived temperature estimates from a core retrieved in the Polar North Atlantic.

The observed preservation indicators show generally high planktic foraminiferal fragmentation and low mean shell weights of *N. pachyderma* and thereby, argue for overall poor preservation conditions (Figure 5A-B). In addition, the generally low $CaCO_3$ record (<30 wt. %) corresponds to earlier findings of low carbonate contents of surface sediments on the Norwegian continental margin associated with poor preservation conditions (Huber et al., 2000) (Figure 5D). At the continental margins, dilution by terrigenous material might lead to low percentages of sedimentary carbonate (Hebbeln et al., 1998), whereas high fertility results in a high input of organic matter and thereby, to enhanced carbonate dissolution (Berger, 1971; Emerson and Bender, 1981; Archer, 1991). Previous studies highlighted that Mg-rich parts might have been removed from the foraminiferal test due to dissolution and thereby, bias the Mg/Ca ratios resulting in underestimated $SST_{Mg/Ca}$ values (Brown and Elderfield, 1996; Rosenthal et al., 2000; Johnstone et al., 2011). Although the risk of measuring biased material was minimized by picking the visually most preserved tests, it remains impossible to quantify the degree of preservation influence on the measured Mg/Ca ratios and hence, the reconstructed $SST_{Mg/Ca}$ and SSS estimates. Due to the observed overall poor preservation conditions, it is likely that the Mg/Ca measurements were influenced by carbonate dissolution.

5.2 Palaeoceanographic evolution of the late Holocene

Throughout the late Holocene, the current proxy records show an overall cooling, with $SST_{Transfer}$ values decreasing from 7.7 to 6.3 °C (Figure 4H; 8C), associated with an overall decreased inflow of Atlantic water. This corresponds well to previous observations of decreased Atlantic water inflow in the Nordic Seas (e.g. Slubowska et al., 2005; Hald et al., 2007; Skirbekk et al., 2010) as well as to lake and tree records from north-western Europe arguing for a late Holocene trend towards colder and dryer conditions (e.g. Bjune et al., 2009; Kaufman et al., 2009). Contrary, at the Vøring plateau south of the study site, planktic

foraminiferal data show an overall increased inflow of Atlantic water throughout this time period (Andersson et al., 2003; Risebrobakken et al., 2003; Andersson et al., 2010). In addition to the overall cooling, the current study also shows smaller scale fluctuations of the sub-surface water masses which will be discussed further for four separate time periods. The interpretation of the fluctuating influence of sub-surface water masses and their possible link with NAO conditions is presented as schematic profiles across the northern Norwegian margin (Figure 9).

5.2.1 Period I: ca. 3500 – 2900 cal yr BP

Between ca. 3500 and 2900 cal yr BP, the relative faunal abundances show increased values of *G. uvula* (ca. 5 to 20 %) and high values (ca. 30 %) of *T. quinqueloba* (Figure 4G; 4C). The latter has been associated with sub-polar conditions and Atlantic water (Bé and Tolderlund, 1971; Volkmann, 2000) and additionally considered to respond rapidly to changes in nutrient supply (Reynolds and Thunnel, 1985; Johannessen et al., 1994). *G. uvula* has been associated with Coastal water and reduced salinities (Husum and Hald, 2012) as well as with high food supplies and cold productive surface waters (e.g. Saito et al., 1981; Boltovskoy et al., 1996; Bergami et al., 2009). Hence, the high relative abundances of both *T. quinqueloba* and *G. uvula* argue for enhanced productivity most likely due to an increased influence of colder, less saline and more productive Coastal water. Additionally, the enriching $\delta^{13}C$ values might also argue for increased primary production corresponding to an increased influence of more productive Coastal water (Figure 6B).

However, the relatively low planktic foraminiferal concentrations and fluxes seem to argue for a rather low primary production (Figure 4A; 5E). These relatively low values might result from relatively poor preservation conditions as indicated by generally high planktic foraminiferal fragmentation, a decreasing mean shell weight of *N. pachyderma* and low $CaCO_3$ values (<22 wt. %) (Figure 5A; 5B; 5D). The latter might reflect the dilution by terrigenous material enhancing carbonate dissolution at the continental margin off Norway (Huber et al., 2000). In addition, the solubility of $CaCO_3$ increases with decreasing temperatures (Edmond and Gieskes, 1970), and thus, the enhanced dissolution conditions are most likely due to a combination of the core location at the continental margin and an increased influence of colder Coastal water.

The depleting $\delta^{18}O$ trend might indicate an increased temperature and/or decreased salinity signal (Figure 6A). The planktic foraminiferal fauna data and decreasing $SST_{Transfer}$ estimates (7.2 to 6.7 °C) with an average value of ca. 6.9 °C argue strongly that the $\delta^{18}O$ record reflects less saline water masses associated with an increased influence of Coastal water (Figure 4H; 8C). Correspondingly, the reconstructed SSS estimates confirm the overall trend towards less saline conditions (Figure 8D). Nonetheless, contrary to decreasing $SST_{Transfer}$ estimations, the overall lower $SST_{Mg/Ca}$ values remain relatively stable throughout this period which might illustrate the different water depths and/or season that the two proxies represent (see section 5.1.3) possibly arguing for more stratified water masses (Figure 8B-C).

Overall, the multi-proxy data argue for an increased influence of Coastal water and possibly more stratified water masses at the core site. This is likely the result of a more westwards located thinning wedge of Coastal water above Atlantic water that might have been the result of a dominating negative NAO-like mode throughout this time interval (Figure 9A). Previously, a 5200 year NAO-index has been reconstructed using a multi-proxy geochemical record from a lake in south-west Greenland (Olsen et al., 2012). Although this NAO-index shows mainly positive values, Olsen et al. (2012) observed a stronger influence of negative NAO conditions between ca. 4500 and 2500 cal yr BP which might correspond to the negative NAO-like conditions suggested here (Figure 8E). Negative NAO conditions are generally associated with a reduced inflow of Atlantic water and a stronger influence of Coastal water (e.g. Sætre, 2007; Hurrell et al., 2013). Correspondingly, between ca. 3500 and 2500 cal yr BP, reconstructed SST estimates from the Vøring plateau (66.58° N, 07.38° E) show decreasing values arguing for a reduced influence of Atlantic water (Andersson et al., 2003; Risebrobakken et al., 2003; Andersson et al., 2010). Additionally, negative NAO conditions result in a colder and dryer climate in north-western Europe (e.g. Wanner et al., 2001). A decreasing temperature and precipitation trend throughout this time interval was observed by pollen and plant macrofossil analyses from a lake record in northern Norway (Svanåvatnet; 66.25° N, 14.03° E) (Bjune and Birks, 2008). Furthermore, based on the mean ablation-season temperature and winter snow accumulation, a decreased winter precipitation was also observed in western Norway (Nesje et al., 2001) and between 3500 and 3200 cal yr BP, a speleothem record from northern Norway indicates decreased surface ground temperatures (Lauritzen and Lundberg, 1999).

5.2.2 Period II: ca. 2900 –1600 cal yr BP

Between ca. 2900 and 1600 cal yr BP, the planktic foraminiferal fauna is characterized by high relative abundances of *T. quinqueloba*, *N. incompta*, *G. glutinata* and *G. bulloides* (Figure 4C-F). These species have all been associated with subpolar conditions and warm Atlantic surface water masses (e.g. Bé and Tolderlund, 1971; Johannessen et al., 1994; Carstens et al., 1997; Simstich et al., 2003) and thus, argue for a pronounced influence of Atlantic water brought to the study area by the NwAC.

The total planktic foraminiferal concentration and flux values show higher and increasing values, especially between ca. 2300 and 1600 cal yr BP, possibly indicating for increased primary production (Figure 4A; 5E). However, the $\delta^{13}C$ record shows an initial depletion towards ca. 2300 cal yr BP followed by relative stable values (ca. 0.3 ‰) arguing for less primary production (Figure 6B). The seemingly increased primary production, reflected by higher flux and concentration, likely results from the generally improved preservation conditions. The observed overall reduced fragmentation and increasing trend of $CaCO_3$ (up to ca. 30 wt. %) argue for a gradual trend towards reduced dissolution conditions throughout this period (Figure 5A; 5D). More favourable preservation conditions have previously been associated with increased influence of Atlantic surface water where pore waters are supersaturated with respect to calcium due to the lower organic matter productivity and a higher rain of $CaCO_3$ (e.g. Huber et al., 2000; Henrich et al., 2002).

The $\delta^{18}O$ record continues its depleting trend from Period I possibly reflecting an increased temperature and/or reduced salinity signal (Figure 6A). The planktic foraminiferal fauna data and the therefrom derived high $SST_{Transfer}$ estimates (ca. 7.3 °C) argue for increasing temperatures which are most likely related to an increased inflow of Atlantic water (Figure 4H; 8C). Correspondingly, the palaeo SSS record shows overall higher values up to ca. 34 ‰ and thus, correlates to an increased influence of more saline Atlantic water (Figure 8D). Additionally, the $SST_{Mg/Ca}$ estimates show, compared to Period I, ca. 0.5 - 1.0 °C higher temperatures associated with an increased influence of Atlantic water (Figure 8B).

The increased influence of Atlantic water inflow suggested here might result from positive NAO conditions. The latter are associated with stronger westerlies across the North Atlantic (e.g. Hurrell et al., 2013). This resulted in an enhanced inflow of Atlantic water which possibly reduced the influence of Coastal water leading to a more eastwards located thinning

wedge of Coastal water above Atlantic water (Figure 9B). Throughout this time period, Olsen et al. (2012) observed a general increasing trend in their NAO-index which might correspond to the influence of a positive NAO mode suggested here **(Figure 8E)**. Similarly high sub-surface temperatures associated with a strengthened inflow of Atlantic water have been observed at the Vøring plateau between ca. 2500 and 1600 cal yr BP (Andersson et al., 2003; Risebrobakken et al., 2003; Andersson et al., 2010). Throughout the time interval of period II, increased temperatures in northern Norway have been observed from a lake record (Bjune and Birks, 2008) and a speleothem record (Lauritzen and Lundberg, 1999). In addition, between ca. 2700 and 1900 cal yr BP increased winter precipitation has been observed in western Norway (Nesje et al., 2001). This correlates well to the warmer and wetter climate scenarios attributed to positive NAO conditions in north-western Europe (e.g. Wanner et al., 2001). Further, the last part of this period might be corresponding to the earlier observed Roman Warm Period between ca. 2000 and 1550 cal yr BP (ca. BCE 50 – CE 400) (Lamb, 1977) and additionally correlate to the findings of warmer temperatures in northern Norway also linked to the Roman Warm Period by Lauritzen and Lundberg (1999).

5.2.3 Period III: ca. 1600 – 950 cal yr BP

Between ca. 1600 and 950 cal yr BP, the planktic foraminiferal fauna shows stable values for all species with particularly high values of *G. uvula* (ca. 25 %) (Figure 4G). This likely reflects a stable period characterized by a strongly increased influence of Coastal water (e.g. Husum and Hald, 2012). At ca. 1600 cal yr BP, both the planktic foraminiferal concentration and flux drop rapidly where after the record remains stable until ca. 950 cal yr BP (Figure 4A; 5E). The planktic foraminiferal fragmentation increases, whereas the $CaCO_3$ record shows an overall decreasing trend (Figure 5A; 5D). This might indicate slightly reduced preservation conditions, possibly related to an enhanced influence of Coastal water and dilution of terrigenous material (e.g. Huber et al., 2000). Correspondingly, the enriched $\delta^{13}C$ record indicates enhanced primary production conditions arguing for a returned influence of Coastal water (Figure 6B).

Although $\delta^{18}O$ values initially continue their decreasing trend towards ca. 1300 cal yr BP, they eventually increase and thereby argue for a possible reduction in temperature (Figure 6A). Compared to Period II, the $SST_{Transfer}$ (ca. 6.6 °C) and $SST_{Mg/Ca}$ records both reflect

stable conditions with ca. 0.5 - 1.0 °C lower estimates indicative of a reduced influence of relatively warm Atlantic water (Figure 8B-C). Additionally, the SSS estimates show a rapid decrease followed by stable, and compared to period II, ca. 0.5 - 1.0 ‰ lower values and thus, also arguing for a reduced influence of Atlantic water or enhanced influence of Coastal water (Figure 8D).

The multi-proxy data argues for a strong influence of Coastal water which is interpreted as a westwards migrated thinning wedge of Coastal water (Figure 9C) which would suggest a shift towards negative NAO conditions (e.g. Sætre, 2007). However, the negative NAO conditions suggested here do not correlate with the overall positive NAO mode reconstructed by Olsen et al. (2012) during this time interval (Figure 8E). The current multi-proxy record corresponds well with other marine and terrestrial observations from nearby the study area within this time interval. Palaeo SST estimates from the Vøring plateau showed a sharp decrease at ca. 1600 cal yr BP where after they remained stable around lower temperatures (compared to values before ca. 1600 cal yr BP) (Andersson et al., 2003; Risebrobakken et al., 2003; Andersson et al., 2010). This also suggests a reduced influence of Atlantic water towards the core site. Further, a colder and dryer climate associated with the Dark Ages was suggested by low surface ground temperatures between ca. 1500 and 900 cal yr BP in northern Norway (e.g. Lauritzen and Lundberg, 1999). Additionally, Bjune and Birks (2008) also observed decreasing air temperatures between ca. 1800 and 800 cal yr BP in northern Norway.

5.2.4 Period IV: ca. 950 – 550 cal yr BP

The increased relative abundance of *N. incompta* indicates a stronger influence of subpolar conditions and thus, a stronger influence of Atlantic water (e.g. Bé and Tolderlund, 1971) (Figure 4D). The concomitant decreasing values of *G. glutinata* and *G. uvula* correspondingly argue for a possible decreased influence of Coastal water (Figure 4E; 4G). The increased abundance of *N. pachyderma* argues for increased polar conditions (e.g. Bé and Tolderlund, 1971; Volkmann, 2000) (Figure 4B). A similar increased abundance of *N. pachyderma* was also found throughout the last ca. 1000 cal yr BP at the Vøring plateau (Risebrobakken et al., 2003). The planktic foraminiferal concentrations and fluxes slightly decrease which might indicate a reduction in primary production (Figure 4A; 5E). Fragmentation and mean shell weight records show a pronounced increase arguing for deteriorated preservation conditions

in the sediment, i.e. increased fragmentation as well as to reduced dissolution of calcite, i.e. increased shell weight (Figure 5A-B). In addition, the $CaCO_3$ record shows a slight increase indicating somewhat reduced dissolution conditions associated with an increased influence of Atlantic water (Huber et al., 2000) (Figure 5D). The increasing $\delta^{13}C$ record might indicate a reduced stratification at the core site resulting from an increased influence of Atlantic water (Figure 6B).

Based on the planktic foraminiferal fauna and the therefrom derived decreasing $SST_{Transfer}$ record, the enriching $\delta^{18}O$ values might reflect a reduced temperature signal (Figure 6A). The $SST_{Transfer}$ record reaches its lowest estimate (ca. 6.3 °C) by the end of the record around ca. 550 cal yr BP (Figure 4H; 8C). The latter contradicts with the previously suggested returned influence of Atlantic water, however, the generally colder temperature estimates are most likely due to the overall cooling trend observed throughout the record and linked to decreasing solar insolation values throughout the late Holocene (e.g. Hald et al., 2007; Kaufman et al., 2009). Nonetheless, contemporaneous reconstructed SST estimates from the Vøring plateau have shown increasing values (Andersson et al., 2003; Risebrobakken et al., 2003; Andersson et al., 2010).

Despite the overall cooling trend, the increased influence of Atlantic water seems to be the result of generally positive NAO conditions (Figure 9D). The reconstructed NAO-index from south-west Greenland also indicate positive NAO conditions during this time interval which are associated with the Medieval Warm Period (Olsen et al., 2012) (Figure 8E). Furthermore, this also corresponds to the results of a NAO reconstruction based on tree rings and speleothems that indicate a dominating positive NAO mode associated with an intensified AMOC (Trouet et al., 2009). These conditions are expressed by a reduced influence of Coastal water and a stronger moisture and heat transport to Norway by the NwAC resulting in warmer and wetter climate conditions (e.g. Wanner et al., 2001; Hurrell et al., 2013). This correlates well to terrestrial records from northern Norway which show slightly increasing air temperatures for this time interval (Bjune and Birks, 2008) and high surface ground temperature estimates between ca. 800 and 500 cal yr BP (Lauritzen and Lundberg, 1999). This time interval most likely reflects the warmer conditions associated with the Medieval Warm Period correlating with observation at the Vøring plateau between ca. 1150 and 650 cal yr BP (ca. 800 – 1300 AD) (Nyland et al., 2006) and in northern Norway between ca. 800 and 500 cal yr BP (ca. 1150 – 1450 AD) (Lauritzen and Lundberg, 1999).

6 Conclusions

A marine core from the northern Norwegian margin was investigated to elucidate the natural variability of water mass properties throughout the late Holocene. In this study, paired Mg/Ca and $\delta^{18}O$ measurements of *N. pachyderma* were presented in order to reconstruct palaeo sub-surface temperature and salinity estimates. Additionally, preservation conditions were analysed and the reconstructed palaeo $SST_{Mg/Ca}$ and SSS estimates were assessed. The palaeoceanographic evolution of the late Holocene was discussed in terms of changing influences of Atlantic and Coastal water and linked to fluctuating modes of the NAO.

The recorded discrepancy between the reconstructed $SST_{Mg/Ca}$ and $SST_{Transfer}$ estimations is likely caused by a combination of several factors such as the restriction of Mg/Ca recordings to a narrow temperature signal, inaccurate estimations of the preferred depth habitat and calcification season of *N. pachyderma* and the initially low Mg/Ca measurements. The overall low measured Mg/Ca ratios might have been influenced by the cleaning method including a reductive step. However, they are likely a direct result of the overall poor preservation conditions associated with the continental margin, resulting in potential underestimations of true $SST_{Mg/Ca}$ and SSS values.

Overall, the proxy results indicate a general cooling trend (7.7 to 6.3 °C, $SST_{Transfer}$) throughout the late Holocene. In addition, fluctuating conditions of Atlantic and Coastal water intensity are observed. Period I (ca. 3500 – 2900 cal yr BP) is influenced by relatively cold (ca. 6.9 °C, $SST_{Transfer}$), less saline and more productive Coastal waters and a stronger vertical stratification of the water column. These conditions are attributed to dominating negative NAO-like conditions. Throughout Period II (ca. 2900 – 1600 cal yr BP), the core site experiences a stronger influence of warm Atlantic water (ca. 7.3 °C, $SST_{Transfer}$) with more favourable preservation conditions associated with positive NAO conditions. The last part of this period likely corresponds to the Roman Warm Period. Within period III (ca. 1600 – 950 cal yr BP), stable conditions and cold sub-surface temperatures (ca. 6.6 °C, $SST_{Transfer}$) are observed indicating a returned and stronger influence of Coastal water. This period correspond very well with the colder and dryer Dark Ages. Period IV (ca. 950 – 550 cal yr BP) experienced a returned stronger influence of Atlantic water attributed to dominating positive NAO conditions and correlates well with the Medieval Warm Period. Nonetheless,

Atlantic water reaching the core site was less warm (ca. 6.3 °C, $SST_{Transfer}$) compared to period II due to the overall late Holocene cooling.

Acknowledgements

This work was carried out within the framework of the Initial Training Network program "Changing Arctic and Subarctic Environments" (CASE, Grant Agreement No. 238111) funded by the European Commission within the 7th Framework Program People, the Research Council of Norway in addition to the University of Tromsø and Norwegian Polar Institute. Jan Sverre Laberg is acknowledged for providing the marine sediment core. Georges Paradis and Dorothy K. Pak are gratefully thanked for cleaning and analysing the Mg/Ca samples at the University of California, Santa Barbara, USA. Additionally, thanks are also extended to Jan P. for his help preparing the maps and Trine Dahl, Julia Sen and Karina Monsen for assisting with laboratory work at the University of Tromsø.

References

Aagaard-Sørensen S, Husum K, Hald M, Marchitto T and Godtliebsen F (2013) Sub sea surface temperatures in the Polar North Atlantic during the Holocene: Planktic foraminiferal Mg/Ca temperature reconstructions. *The Holocene* 24(1): 93-103.

Aksu AE and Vilks G (1988) Stable isotopes in planktonic and benthic foraminifera from Arctic Ocean surface sediments. *Can. J. Earth Sci.* 25: 701-709.

Andersson C, Risebrobakken B, Jansen E and Dahl SO (2003) Late Holocene surface ocean conditions of the Norwegian Sea (Voring Plateau). *Paleoceanography* 18: PA1044, doi: 10.1029/2001PA000654.

Andersson C, Pausata FSR, Jansen E, Risebrobakken B and Telford RJ (2010) Holocene trends in the foraminifer record from the Norwegian Sea and the North Atlantic Ocean. *Clim. Past* 6: 179-193.

Archer D (1991) Modeling the calcite lysocline. *J. Geophys. Res.* 96(C9): 17037-17050.

Aspeli R (1994) Late Quaternary benthic foraminiferal stratigraphy on the western Barents slope Sea. Unpublished thesis, University of Tromsø (in Norwegian).

Barker S and Elderfield H (2002) Foraminiferal calcification response to glacial interglacial changes in atmospheric CO_2. *Science* 297: 883-836.

Barker S, Greaves M and Elderfield H (2003) A study of cleaning procedures used for foraminiferal Mg/Ca paleothermometry. *Geochem. Geophys. Geosyst.* 4(9): 8407, doi:10.1029/2003GC000559.

Barker S, Kiefer T and Elderfield H (2004) Temporal changes in North Atlantic circulation constrained by planktonic foraminiferal shell weights. *Paleoceanography* 19: PA3008.

Bauch D, Carstens J, Wefer G and Thiede J (2000) The imprint of anthropogenic CO_2 in the Arctic Ocean: evidence from planktic $d^{13}C$ data from water column and sediment surfaces. *Deep-Sea Res. Pt. II* 9(11): 1791–1808.

Bé AWH and Tolderlund DS (1971) Distribution and ecology of living planktonic foraminifera in surface waters of the Atlantic and Indian Oceans. In: Funnell BM and Riedel WR (eds) *The Micropaleontology of the Oceans*. Cambridge University Press, London, 105-149.

Beer CJ, Schiebel R and Wilson PA (2010) Testing planktic foraminiferal shell weight as a surface water [CO_3^{2-}] proxy using plankton net samples. *Geology* 38: 103-106.

Berben SMP, Husum K, Cabedo-Sanz P and Belt ST (2014) Holocene sub-centennial evolution of Atlantic water inflow and sea ice distribution in the western Barents Sea. *Clim. Past* 10: 181-198, doi:10.5194/cp-10-181-2014.

Bergami C, Capotondi L, Langone L, Giglio F and Ravaioli M (2009) Distribution of living planktonic foraminifera in the Ross Sea and the Pacific sector of the Southern Ocean (Antarctica). *Mar. Micropaleontol.* 73: 37-48.

Berger WB (1971) Sedimentation of planctonic foraminifera. *Mar. Geol.* 11: 325-358.

Bjune AE and Birks HJB (2008) Holocene vegetation dynamics and inferred climate changes at Svanåvatnet, Mo i Rana, northern Norway. *Boreas* 37: 146-156.

Bjune AE, Seppä H and Birks HJB (2009) Quantitative summer temperature reconstructions for the last 2000 years based on pollen-stratigraphical data from northern Fennoscandia. *J. Paleolimnol.* 41: 43-56.

Blaume F (2002) Physical oceanography from CTD PO181_311. doi:10.1594/PANGAEA.77314.

Boltovskoy E, Boltovskoy D, Correa N and Brandini F (1996) Planktic foraminifera from the southwestern Atlantic (30° – 60°S): Species-specific patterns in the upper 50 m. *Mar. Micropaleontol.* 28: 53–72.

Boyle EA (1983) Manganese carbonate overgrowths on foraminifera tests. *Geochim. Cosmochim. Acta* 47: 1815-1819.

215,000 years: Changes in deep ocean circulation and chemical inventories. *Earth Planet. Sci. Lett.* 76: 135-150.

Broecker WS and Clark E (2001) An evaluation of Lohmann's foraminifera weight dissolution index. *Paleoceanography* 16: 531-534.

Brown SJ and Elderfield H (1996) Variations in Mg/Ca and Sr/Ca ratios of planktonic foraminifera caused by postdepositional dissolution: Evidence of shallow Mg-dependent dissolution. *Paleoceanography* 11(5): 543-551.

Bryson RA and Goodman BM (1980) Volcanic activity and climate change. *Science* 207: 1041-1044.

Carstens J, Hebbeln D and Wefer G (1997) Distribution of planktic foraminifera at the ice margin in the Arctic (Fram Strait). *Mar. Micropaleontol.* 29: 257-269.

Cifelli R (1961) Globigerina incompta, a new species of pelagic foraminifera from the North Atlantic. Contributions Cushman Foundation Foraminiferal Research 12: 83-86.

Conan SMH, Ivanova EM and Brummer GJA (2002) Quantifying carbonate dissolution and calibration of foraminiferal dissolution indices in the Somali Basin. *Mar. Geol.* 182: 325-349.

Darling KF, Kucera M, Kroon D and Wade CM (2006) A resolution for the coiling direction paradox in Neogloboquadrina pachyderma. *Paleoceanography* 21: PA2011, doi:10-1029/2005PA001189.

Dekens PS, Lea DW, Pak DK and Spero HJ (2002) Core top calibration of Mg/Ca in tropical foraminifera: Refining paleotemperatures estimation. *Geochem. Geophys. Geosyst.* 3(4): 1022, doi:10.1029/2001GC000200.

Donner B and Wefer G (1994) Flux and stable isotope composition of Neogloboquadrina pachyderma and other planktonic foraminifers in the Southern Ocean (Atlantic sector). *Deep-Sea Res. Pt. I* 41: 1733-1743.

Duplessy JC, Ivanova E, Murdmaa I, Paterne M and Labeyrie L (2001) Holocene paleoceanography of the northern Barents Sea and variations of the northward heat transport by the Atlantic Ocean. *Boreas* 30: 2-16.

Edmond JM and Gieskes TM (1970) On the calculation of the degree of saturation of sea water with respect to calcium carbonate under in situ conditions. *Geochim. Cosmochim. Acta* 35: 1261-1291.

Ehrmann WU and Thiede J (1985) History of Mesozoic and Cenozoic sediment fluxes to the North Atlantic Ocean. Contributions to Sedimentology E. Schweizerbart'sche Verlagsbuchhandlung, Stuttgart, 15: 1-109, ISBN 3-510-57015-4.

Elderfield H and Ganssen G (2000) Past temperature and d18O of surface ocean waters inferred from foraminiferal Mg/Ca ratios. *Nature* 405: 442-445, doi:10.1038/35013033.

Elderfield H, Vautravers M and Cooper M (2002) The relationship between shell size and Mg/Ca, Sr/Ca, δ18O, and δ13C of species of planktonic foraminifera. *Geochem. Geophys. Geosyst.* 3(8): 1-13.

Elderfield H, Greaves M, Barker S, Hall IR, Tripati A, Ferretti P, Crowhurst S, Booth L and Daunt C (2010) A record of bottom water temperature and seawater [delta]18O for the Southern Ocean over the past 440 kyr based on Mg/Ca of benthic foraminiferal Uvigerina spp. *Quaternary Sci. Rev.* 29: 160-169.

Emerson S and Bender M (1981) Carbon fluxes at the sediment-water interface of the deep-sea: calcium carbonate preservation. *J. Mar. Res.* 39: 139-162.

Espitalié J, Laporte JL, Madec M, Marquis F, Leplat P, Paulet J and Boutefeu A (1977) Méthode rapide de characterisation des roches-mere, de leur potential petrolier et de leur degre d'évolution. *Revue de l'Institute Francais du Petrole* 32: 23-42.

Giraudeau J, Jennings AE and Andrews JT (2004) Timing and mechanisms of surface and intermediate water circulation changes in the Nordic seas over the last 10,000 cal years: A view from the north Iceland shelf. *Quaternary Sci. Rev.* 23: 2127-2139.

Hald M, Andersson C, Ebbesen H, Jansen E, Klitegaard-Kristensen D, Risebrobakken B, Salomonsen GR, Sejrup HP, Sarnthein M and Telford R (2007) Variations in temperature and extent of Atlantic water in the northern North Atlantic during the Holocene. *Quaternary Sci. Rev.* 26: 3423-3440.

Hebbeln C, Henrich R and Baumann KH (1998) Paleoceanography of the last glacial/interglacial cycle in the Polar North Atlantic. *Quat. Sci. Rev.* 17: 125-153.

Hemleben C, Spindler M and Anderson OR (1989) Modern planktonic foraminifera. Springer, New York, 363.

Henrich R, Baumann KH, Huber R and Meggers H (2002) Carbonate preservation records of the past 3Myr in the Norwegian-Greenland Sea and the northern North Atlantic: Implications for the history of NADW production. *Mar. Geol.* 184: 17-39.

Hopkins TS (1991) The GIN Sea: A synthesis of its physical oceanography and literature review, 1972–1985. *Earth Sci. Rev.* 30: 175-318.

Huber R, Meggers H, Baumann KH and Henrich R (2000) Recent and Pleistocene carbonate dissolution in sediments of the Norwegian-Greenland Sea. *Mar. Geol.* 165: 123-136.

Hurrell JW, Kushnir Y, Ottersen G and Visbeck M (2013) An overview of the North Atlantic Oscillation. The North Atlantic Oscillation: Climatic significance and environmental impact. American Geophysical Union, 1-35.

Husum K and Hald M (2012) Arctic planktic foraminiferal assemblages: Implications for subsurface temperature reconstructions. *Mar. Micropaleontol.* 96(97): 38-47.

Hut G (1987) Stable isotope reference samples for geochemical and hydrological investigations. paper presented at Consultants Group Meeting, Int. At. Energy Agency, Vienna.

Ikeda M, Johannessen JA, Lygre K and Sandven S (1989) A process study of mesoscale meanders and eddies in the Norwegian Coastal Current. *J. Phys. Oceanogr.* 19: 20-35.

Jernas P, Klitgaard Kristensen D, Husum K, Wilson L and Koç N (2013) Palaeoenvironmental changes of the last two millennia on the western and northern Svalbard shelf. *Boreas* 42: 236-255.

Jiang H, Eiriksson J, Schulz M, Knudsen KL, Seidenkrantz MS (2005) Evidence for solar forcing of sea-surface temperature on the North Icelandic Shelf during the Late Holocene. *Geology* 33(1): 73-76.

Johannessen T, Jansen E, Flatøy A and Ravelo AC (1994) The relationship between surface water masses, oceanographic fronts and plaeoclimatic proxies in surface sediments of the Greenland, Iceland, Norwegian Seas. In: Zahn R, Pedersen TF, Kaminski MA and Labeyrie L (eds) *Carbon Cycling in the Glacial Ocean: Constraints of the Ocean's Role in Global Change*. Berlin, Springer, 61-86.

Johnstone HJH, Yu J, Elderfield H and Schulz M (2011) Improving temperature estimates derived from Mg/Ca of planktonic foraminifera using X-ray computed tomography-based dissolution index, XDX. *Paleoceanography* 26(1): PA1215, DOI: 10.1029/2009pa001902.

Jonkers L, Brummer GJA, Peeters FJC, van Aken HM and De Jong MF (2010) Seasonal stratification, shell flux, and oxygen isotope dynamics of left-coiling N. pachyderma and T. quinqueloba in the western sub polar North Atlantic. *Paleoceanography* 25: PA2204.

Jonkers L, Jiménez-Amat P, Graham Mortyn P and Brummer GJA (2013) Seasonal Mg/Ca variability of N. pachyderma (s) and G. bulloides: Implications for seawater temperature reconstruction. *Earth Planet. Sci. Lett.* 376: 137-144.

Juggins S (2010) C2 1.7.2 available at http://www.staff.ncl.ac.uk/staff/stephen.juggins/.

Kaufman DS, Schneider DP, McKay NP, Ammann CM, Bradley RS, Briffa KR, Miller GH, Otto-Bliesner BL, Overpeck JT, Vinther BM and Arctic Lakes 2k Project Members (2009) Recent warming reverses long-term Arctic cooling. *Science* 325: 1236-1239.

Keigwin LD and Boyle EA (1989) Late Quaternary paleochemistry of high-latitude surface waters. *Palaeogeogr. Palaeocl.* 73: 85-106.

Knudsen KL (1998) Foraminiferer i Kvartær stratigrafi: Laboratorie og fremstillingsteknik samt udvalgte eksempler. *Geologisk Tidsskrift* 3: 1-25.

Kohfeld KE, Fairbanks RG and Smith SL (1996) *Neogloboquadrina pachyderma* (sinistral coiling) as paleoceanographic tracers in polar oceans: Evidence from northeast water polynya plankton tows, sediments traps, and surface sediments. *Paleoceanography* 11: 679-699.

Kozdon R, Eisenhauer A, Weinelt M, Meland MY and Nuernberg D (2009) Reassessing Mg/Ca temperature calibrations of Neogloboquadrina pachyderma (sinistral) using paired d44/40Ca and Mg/Ca measurements. *Geochem. Geophys. Geosyst.* 10: Q03005, doi:10.1029/2008GC002169.

Laberg JS, Vorren TO, Mienert J, Bryn P and Lien R (2002) The Trænadjupet slide: a large slope failure affecting the continental margin of Norway 4,000 years ago. *Geo. Mar. Lett.* 22: 19-24.

Lamb HH (1977) Climate, Present, Past and Future. Volume 2. Climatic History and the Future. Methuen & Co Ltd, London, 835.

Lauritzen SE and Lundberg J (1999) Calibration of the speleothem delta function: an absolute temperature record for the Holocene in northern Norway. *The Holocene* 9(6): 650-669.

Le J and Shackleton NJ (1992) Carbonate dissolution fluctuations in the western equatorial Pacific during the late Quaternary. *Paleoceanography* 7: 21-42.

Lea DW, Mashiotta TA and Spero HJ (1999) Controls on magnesium and strontium uptake in planktonic foraminifera determined by live culturing. *Geochim. Cosmochim. Acta* 63: 2369-2379.

Lean J (2002) Solar forcing of climate change in recent millennia. In: Wefer G, Berger WH, Behre KE and Jansen E (eds) *Climate development and history of the North Atlantic realm*. Berlin, Springer-Verlag, 75-88.

Lubinski DJ, Polyak L and Forman SL (2001) Freshwater and Atlantic water inflows to the deep northern Barents and Kara seas since ca 13 ^{14}Cka: foraminifera and stable isotopes. *Quaternary Sci. Rev.* 20: 1851-1879.

Mangerud J, Bondevik S, Gulliksen S, Hufthammer AK and Høisæter T (2006) Marine ^{14}C reservoir ages for 19th century whales and molluscs from the North Atlantic. *Quaternary Sci. Rev.* 25: 3228-3245.

Mashiotta TA, Lea DW and Spero HJ (1999) Glacial interglacial changes in Subantarctic sea surface temperature and d18O-water using foraminiferal Mg. *Earth Planet. Sci. Lett.* 170: 417-432, doi:10.1016/S0012-821X(99)00116-8.

Meland MY, Jansen E, Elderfield H, Dokken TM, Olsen A and Bellerby RGJ (2006) Mg/Ca ratios in the planktonic foraminifer Neogloboquadrina pachyderma (sinistral) in the northern North Atlantic/Nordic seas. *Geochem. Geophys. Geosyst.* 7: Q06P14, doi:10.1029/2005GC001078.

Nesje A, Matthews JA, Dahl SO, Berrisford MS and Andersson C (2001) Holocene glacier fluctuation of Flatebreen and winter-precipitation changes in the Jostedalsbreen region, western Norway, based on glaciolacustrine sediment records. *The Holocene* 11: 267–280.

Nürnberg D (1995) Magnesium in tests of Neogloboquadrina pachyderma sinistral from high northern and southern latitudes. *J. Foraminiferal Res.* 25(4): 350-368.

Nürnberg D, Bijma J and Hemleben C (1996) Assessing the reliability of magnesium in foraminiferal calcite as a proxy for water mass temperatures. *Geochim. Cosmochim. Acta* 60: 803-814, doi:10.1016/0016-7037(95)00446-7.

Nyland B, Jansen E, Elderfield H and Andersson C (2006) Neogloboquadrina pachyderma (dex. and sin.) Mg/Ca and d18O records from the Norwegian Sea. *Geochem. Geophys. Geosyst.* 7: Q10P17, doi:10.1029/2005GC001055.

O'Neil JR, Clayton RN and Mayeda TK (1969) Oxygen isotope fractionation in divalent metal carbonates. *J. Chem. Phys.* 51(12): 5547-5558, doi:10.1063/1.1671982.

Olsen J, Anderson NJ and Knudsen MF (2012) Variability of the North Atlantic Oscillation over the past 5200 years. *Nature Geoscience* 5: 808-812. 28 July 2014, ftp://ftp.ncdc.noaa.gov/pub/data/paleo/paleolimnology/greenland/lake-ss1220-2012.xls.

Oppo DW and Fairbanks RG (1989) Carbon isotope composition of tropical surface water during the past 22,000 years. *Paleoceanography* 4: 333-351.

Orvik KA and Niiler P (2002) Major pathways of Atlantic water in the northern North Atlantic and Nordic Seas toward Arctic. *Geophys. Res. Lett.* 29(19): 1896, doi:10.1029/2002GL015002.

Ottersen G, Planque B, Belgrano A, Post E, Reid P and Stenseth N (2001) Ecological effects of the North Atlantic Oscillation. *Oecologia* 128: 1-14.

Perkins H, Hopkins TS, Malmberg SA, Poulain PM and Warn-Varnas A (1998) Oceanographic conditions east of Iceland. *J. Geophys. Res.* 103: 21531-21542.

Pufhl HA and Shackleton NJ (2004) Two proximal, high-resolution records of foraminiferal fragmentation and their implications for changes in dissolution. *Deep-Sea Res. Pt. I* 51: 809-832.

Rasmussen TL and Thomsen E (2010) Holocene temperature and salinity variability of the Atlantic Water inflow to the Nordic Seas. *The Holocene* 20(8): 1223-1234.

Reimer PJ, Bard E, Bayliss A, Beck JW, Blackwell PG, Ramsey CB, Buck CE, Cheng H, Edwards RL, Friedrich M, Grootes PM, Guilderson TP, Haflidason H, Hajdas I, Hatté C, Heaton TJ, Hoffmann DL, Hogg AG, Hughen KA, Kaiser KF, Kromer B, Manning SW, Niu M, Reimer RW, Richards DA, Scott EM, Southon JR, Staff RA, Turney CSM and van der Plicht J (2013) Intcal13 and Marine13 radiocarbon age calibration curves. *Radiocarbon* 55(4): 1869-1887.

Reynolds L and Thunnel RC (1985) Seasonal succession of planktonic foraminifera in the subpolar North Pacific. *J. Foramin. Res.* 15: 282-301.

Risebrobakken B, Jansen E, Mjele E and Hevrøy K (2003) A high resolution study of Holocene paleoclimatic and paleoceanographic changes in the Nordic Seas. *Paleoceanography* 18: 1017, doi:10.1029/2002PA000764.

Risebrobakken B, Morros M, Ivanova EV, Chistyakova N and Rosenberg R (2010) Climate and oceanographic variability in the SW Barents Sea during the Holocene. *Holocene* 20: 609-621.

Rørvik KL, Laberg JS, Hald M, Ravna EK and Vorren TO (2010) Behavior of the northwestern part of the Fennoscandian ice sheet during the Last Glacial Maximum – a response to external forcing. *Quaternary Sci. Rev.* 29: 2224-2237.

Rosenthal Y, Lohmann GP, Lohmann KC and Sherrell RM (2000) Incorporation and preservation of Mg in *Globigerinoides sacculifer*: Implications for reconstructing the temperature and 18O/16O of seawater. *Paleoceanography* 15(1): 135-145.

Sætre R (2007) The Norwegian coastal current. Tapir academic press, Trondheim, 89-99.

Saito T, Thompson PR and Breger D (1981) Systematic index of recent and pleistocene planktonic foraminifera. University of Tokyo press, Tokyo, 1-190.

Sarnthein M, Van Kreveld S, Erlenkeuser H, Grootes PM, Kucera M, Pflaumann U and Schulz M (2003) Centennial-to-millennial-scale periodicities of Holocene climate and sediment injections off the western Barents shelf, 75 °N. *Boreas* 32: 447-461.

Shackleton NJ (1974) Attainment of isotopic equilibrium between ocean water and the benthonic foraminifera genus uvigerina: Isotopic changes in the ocean during the last glacial. *Colloq. Int. CNRS* 219: 203-209.

Simstich J, Sarnthein M and Erlenkeuser H (2003) Paired δ18O signals of N. pachyderma (s) and T. quinqueloba show thermal stratification structure in the Nordic seas. *Mar. Micropaleontol.* 48: 107–125.

Skirbekk K, Klitgaard Kristensen D, Rasmussen TL, Koç N and Forwick M (2010) Holocene climate variations at the entrance to a warm Arctic fjord: evidence from Kongsfjorden trough, Svalbard. *Geological society, London, Special Publications*, 344: 289-304, doi:10.1144/SP344.20.

Slubowska MA, Koç N, Rasmussen TL and Klitgaard-Kristensen D (2005) Changes in the flow of Atlantic water into the Arctic Ocean since the last deglaciation: Evidence from the northern Svalbard continental margin, 80N. *Paleoceonography* 20: PA4014, doi:10.1029/2005PA001141.

Slubowska-Woldengen M, Rasmussen TL, Koç N, Klitgaard-Kristensen D, Nilsen F and Solheim A (2007) Advection of Atlantic Water to the western and northern Svalbard shelf since 17 500 cal yr BP. *Quaternary Sci. Rev.* 26: 463-478.

Solignac S, Giraudeau J and De Vernal A (2006) Holocene sea surface conditions in the western North Atlantic: Spatial and temporal heterogeneities. *Paleoceanography* 21: PA2004, doi:10.1029/2005PA001175.

Stangeew E (2001) Distribution and isotopic composition of living planktonic foraminifera N. pachyderma (sinistral) and T. quinqueloba in the high latitude North Atlantic. Ph.D. thesis, Math.-Naturwiss. Fak., Christian-Albrechts-Univ., Kiel, Germany. (Available at http://e-diss.uni-kiel.de/diss_464/pp).

Stuiver M and Reimer PJ (1993) Extended 14C data base and revised CALIB 3.0 14C age calibration program. *Radiocarbon* 35: 215-230.

Telford RJ and Birks HJB (2005) The secret assumption of transfer functions: Problems with spatial autocorrelation in evaluating model performance. *Quaternary Sci. Rev.* 24: 2173-2179.

Ter Braak CJF and Juggins S (1993) Weighted averaging partial least squares regression (WA-PLS): An improved method for reconstructing environmental variables from species assemblages. *Hydrobiologia* 269(270): 485-502.

Thornalley DJR, Elderfield H and McCave IN (2009) Holocene oscillations in temperature and salinity of the surface subpolar North Atlantic. *Nature* 457: 711-714.

Trouet V, Esper J, Graham NE, Baker A, Scourse JD and Frank DC (2009) Persistent positive North Atlantic Oscillation mode dominated the Medieval Climate Anomaly. *Science* 324: 78-80.

Volkmann R (2000) Planktic foraminifers in the outer Laptev Sea and the Fram Strait: Modern distribution and ecology. *J. Foramin. Res.* 30: 157-176.

Wanner H, Brönnimann S, Casty C, Gyalistras D, Luterbacher J, Schmutz C, Stephenson D and Xoplaki E (2001) North Atlantic Oscillation – Concepts and studies. *Surveys in Geophysics* 22: 321-381.

Wanner H, Beer J, Bütikofer J, Crowley TJ, Cubasch U, Flückiger J, Goosse H, Grosjean M, Joos F, Kaplan JO, Küttel M, Müller SA, Prentice IC, Solomina O, Stocker TF, Tarasov P, Wagner M and Widmann M (2008) Mid- to Late Holocene climate change: an overview. *Quaternary Sci. Rev.* 27(19-20): 1-38, doi:10.1016/j.quascirev.2008.06.013.

Werner K, Spielhagen RF, Bauch D, Hass HC and Kandiano E (2013) Atlantic Water advection versus sea-ice advances in the eastern Fram Strait during the last 9 ka: Multiproxy evidence for a two-phase Holocene. *Paleoceanography* 28: 283-295.

Zamelczyk K, Rasmussen TL, Husum K and Hald M (2013) Marine calcium carbonate preservation vs. climate change over the last two millennia in the Fram Strait: Implications for planktic foraminiferal paleostudies. *Mar. Micropaleontol.* 98: 14-27.

Figure captions

Table 1: AMS ^{14}C dates and calibrated radiocarbon ages of W00-SC3. The calibration is performed using Calib 7.0.0 software (Stuiver and Reimer, 1993), the Marine13 calibration curve (Reimer et al., 2013) and a local reservoir age (ΔR value) of 71 ± 21 following Mangerud et al. (2006). The AMS ^{14}C date highlighted in grey is omitted from the final depth-age model.

Table 2: Planktic foraminiferal species list.

Figure 1: Study area of W00-SC3 (67.24° N, 08.31° E) (green) with the main surface currents: Norwegian Atlantic Current (NwAC) (red) and Norwegian Coastal Current (NCC) (black). A) Surface currents presented on a bathymetric map. B) Generalized schematic profile across the northern Norwegian margin modified after Rørvik et al. (2010). Coastal water (CW), Atlantic water (AW), Atlantic intermediate water (AIW) and Deep water (DW). C) Detail map of the surface currents nearby the core site modified after Sætre (1983). Red and black arrows indicate Atlantic and Coastal water respectively.

Figure 2: CTD data from PO181_311 (67.10° N, 08.26° E) (Blaume, 2002). Temperature (black) and salinity (grey) versus water depth. Atlantic water mass is highlighted in grey.

Figure 3: Depth-age model of W00-SC3 based on three calibrated AMS ^{14}C dates. The 2-σ range of the calibrated radiocarbon ages is indicated by an error bar. The exact values are noted in black for the used dates and grey for one omitted AMS ^{14}C date. A) Calibrated calendar years BP versus core depth. B) Sedimentation rates versus core depth.

Figure 4: Planktic foraminiferal fauna versus cal yr BP (left y-axis) and cal yr BCE/CE (right y-axis). The black diamonds on the Y-axis indicate the AMS ^{14}C converted to calibrated radiocarbon ages. The horizontal lines (grey) in the background indicate the boundaries between the different periods. A) Planktic foraminiferal concentration (black) and flux (grey) versus age. B-G) Species-specific relative abundances (black) and fluxes (grey) of planktic foraminifera versus age. H) Transfer function derived $SST_{Transfer}$ estimates using a modern foraminiferal dataset by Husum and Hald (2012) versus age.

Figure 5: Preservation and geochemical analysis versus cal yr BP (left y-axis) and cal yr BCE/CE (right y-axis). The black diamonds on the Y-axis indicate the AMS ^{14}C converted to calibrated radiocarbon ages. The horizontal lines (grey) in the background indicate the boundaries between the different periods. A) Planktic foraminiferal fragmentation versus age. B) Mean shell weight of *N. pachyderma* versus age. C) Total organic carbon versus age. D) Calcium carbonate versus age. E) Planktic foraminiferal concentration (black) and flux (grey) versus age.

Figure 6: Stable isotopes analysis performed on *N. pachyderma* versus cal yr BP (left y-axis) and cal yr BCE/CE (right y-axis). The black diamonds on the Y-axis indicate the AMS ^{14}C converted to calibrated radiocarbon ages. The horizontal lines (grey) in the background indicate the boundaries between the different periods. A) $\delta^{18}O$ measurements corrected for a vital effect of 0.6 ‰ according Simstich et al. (2003) and Nyland et al. (2006) versus age. B) $\delta^{13}C$ measurements versus age.

Figure 7: Trace element analysis plotted as correlations of contamination tracers versus Mg/Ca ratios. A-C) Correlations are plotted for all measurements. D-F) Samples with ratios higher than 100 µmol/mol are omitted following the contamination threshold of Barker et al. (2003). A; D) Fe/Ca versus Mg/Ca. B; E) Al/Ca versus Mg/Ca. C;F) Mn/Ca versus Mg/Ca.

Figure 8: Water mass properties versus cal yr BP (left y-axis) and cal yr BCE/CE (right y-axis). The black diamonds on the Y-axis indicate the AMS ^{14}C converted to calibrated radiocarbon ages. The horizontal lines (grey) in the background indicate the boundaries between the different periods. A) Mg/Ca ratios of *N. pachyderma* versus age. B) $SST_{Mg/Ca}$ estimates obtained by the temperature:Mg/Ca equation of Kozdon et al. (2009) versus age. C) $SST_{Transfer}$ estimates using the modern foraminiferal dataset by Husum and Hald (2012) versus age. D) SSS estimates derived by a combined $\delta^{18}O_c$ and $SST_{Mg/Ca}$ approach using the salinity to $\delta^{18}O_w$ relation for the central and eastern Nordic Seas by Simstich et al. (2003) versus age. E) Reconstructed NAO-index from a lake record in south-west Greenland (Olsen et al., 2012) versus age.

Figure 9: The interpretation of fluctuating influence of sub-surface water masses based on multi-proxy data from the study area is presented as a schematic profile across the northern Norwegian margin for four separate time periods. Coastal water (CW), Atlantic water (AW), Atlantic intermediate water (AIW) and Deep water (DW).

Table 1

Lab ID	Core depth (cm)	Material	Uncorrected ^{14}C age	cal yr BP	2-σ range BP	cal yr BCE/CE	2-σ range BCE/CE	Reference
Beta-334422	23.5	*N. pachyderma*	1590 ± 30	1069	968 - 1170	881 CE	780 - 982 CE	This study
TUa-2931	40.0	*N. pachyderma*	1360 ± 65	821.5	684 - 959	1128.5 CE	991 - 1266 CE	Laberg et al., 2002
TUa-2930	120.0	*N. pachyderma*	2305 ± 55	1836	1688 - 1984	114.5 CE	35 BC - 262 CE	Laberg et al., 2002
TUa-2929	263.0	*N. pachyderma*	3660 ± 95	3484.5	3237 - 3732	1535.5 BCE	1783 - 1288 BCE	Laberg et al., 2002

Table 2

Planktic foraminiferal species
Globigerina bulloides (d'Orbigny), 1826
Globigerinita glutinata (Egger), 1893
Globigerinita uvula (Ehrenberg), 1861
Neogloboquadrina incompta (Cifelli), 1961
Neogloboquadrina pachyderma (sinistral) (Ehrenberg), 1861
Turborotalita quinqueloba (Natland), 1838

Figure 1

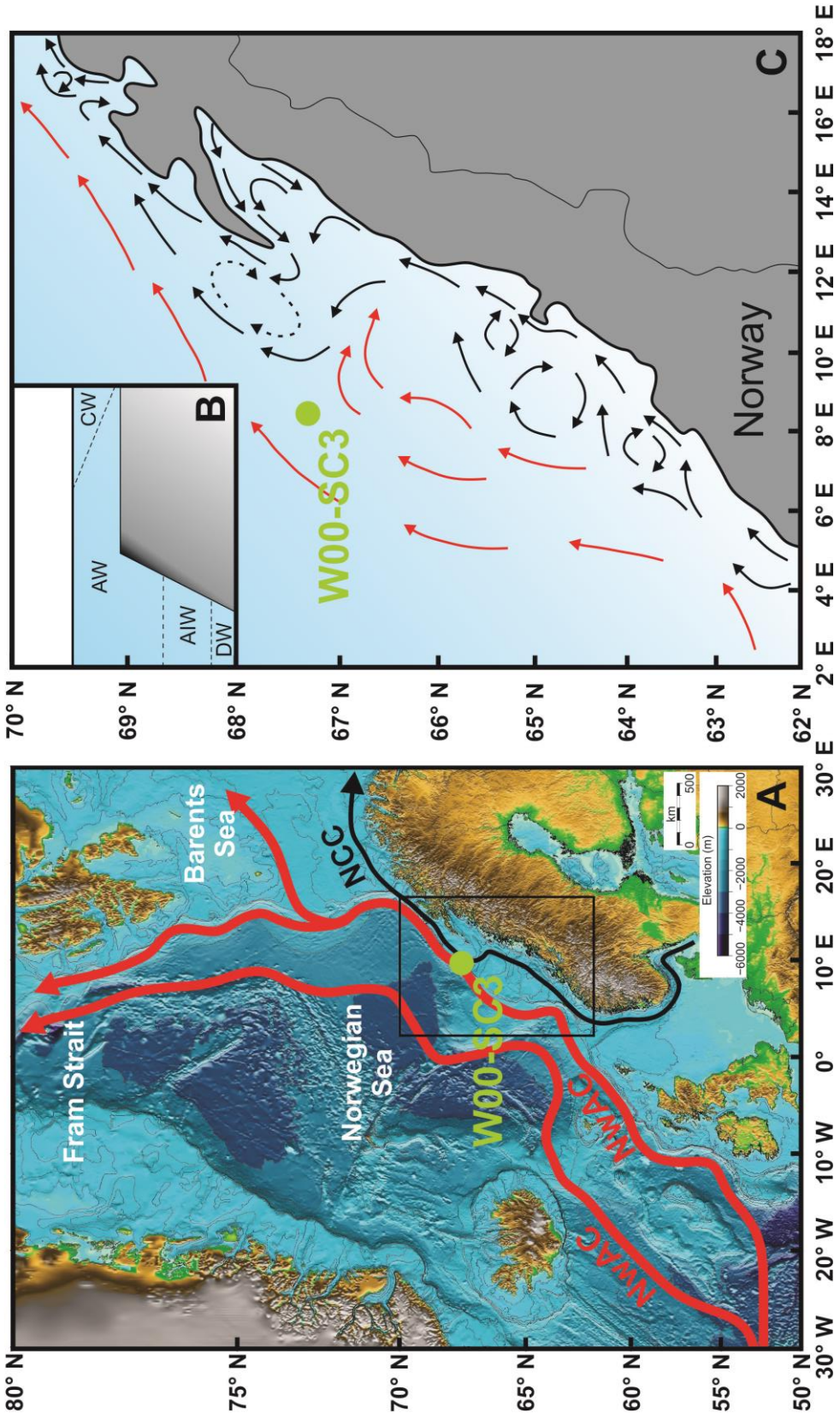
A
B
C
Fram Strait
Barents Sea
Norwegian Sea
NCC
W00-SC3
NwAC
NwAC
W00-SC3
Elevation (m)
km
AW
AIW
DW
CW
Norway
80° N
75° N
70° N
65° N
60° N
55° N
50° N
30° W
20° W
10° W
0°
10° E
20° E
30° E
70° N
69° N
68° N
67° N
66° N
65° N
64° N
63° N
62° N
2° E
4° E
6° E
8° E
10° E
12° E
14° E
16° E
18° E

Figure 2

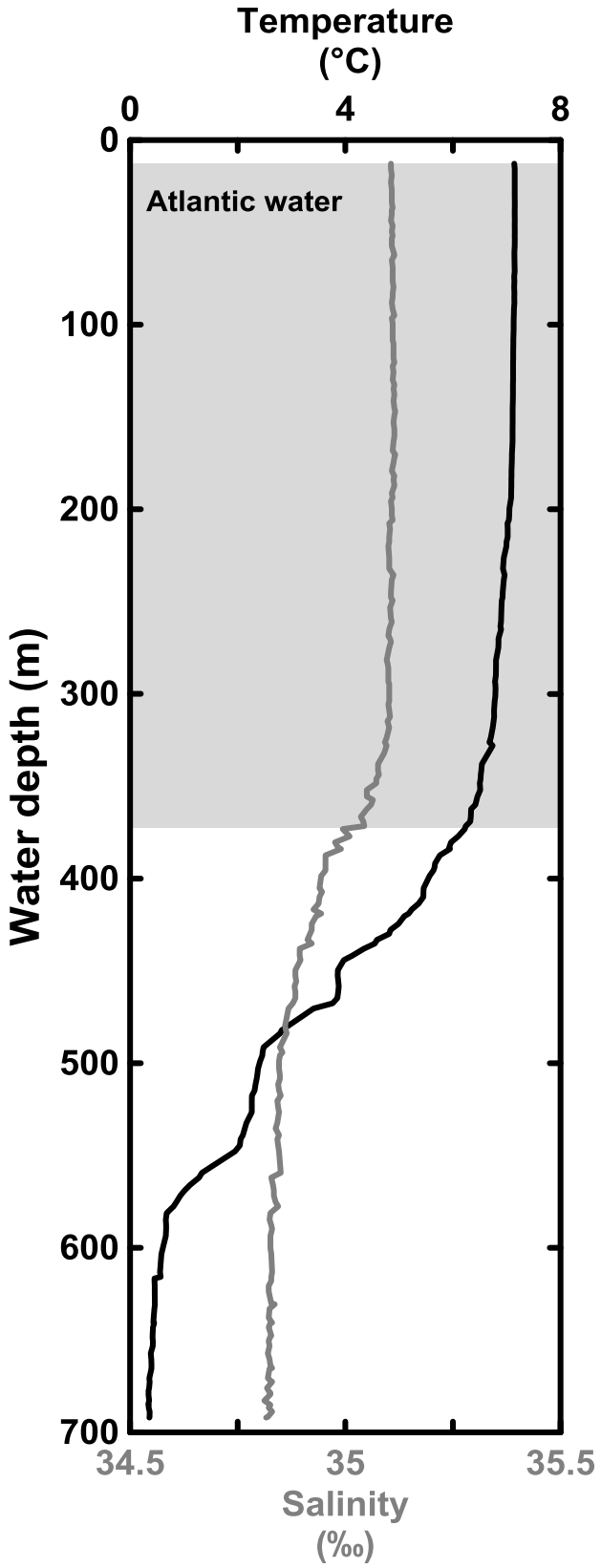
Temperature
(°C)
0
4
8
0
Atlantic water
100
200
300
400
500
600
700
Water depth (m)
34.5
35
35.5
Salinity
(‰)

Figure 3

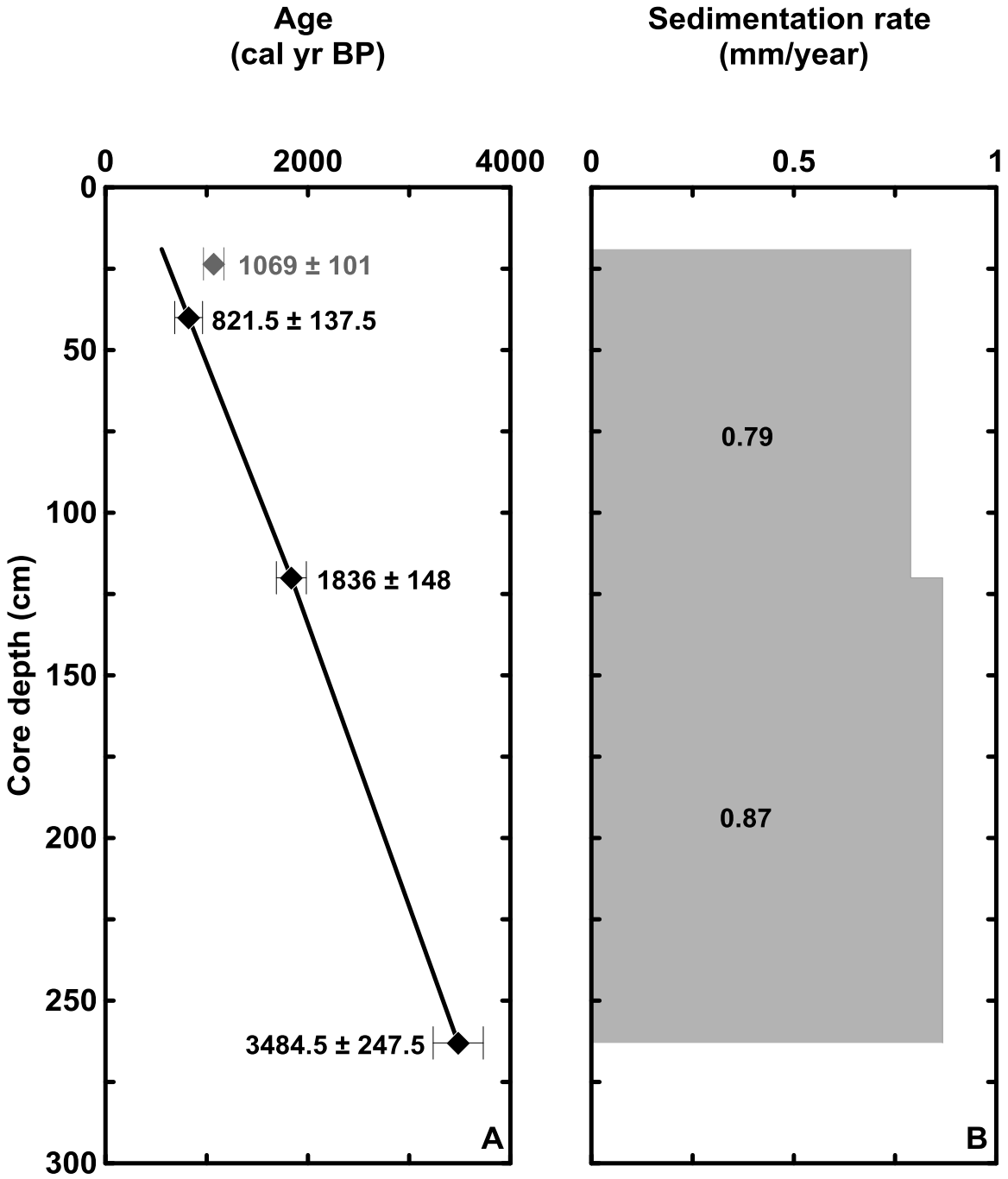
Age
(cal yr BP)
Sedimentation rate
(mm/year)
0
2000
4000
0
0.5
1
Core depth (cm)
0
50
100
150
200
250
300
1069 ± 101
821.5 ± 137.5
1836 ± 148
3484.5 ± 247.5
0.79
0.87
A
B

Figure 4

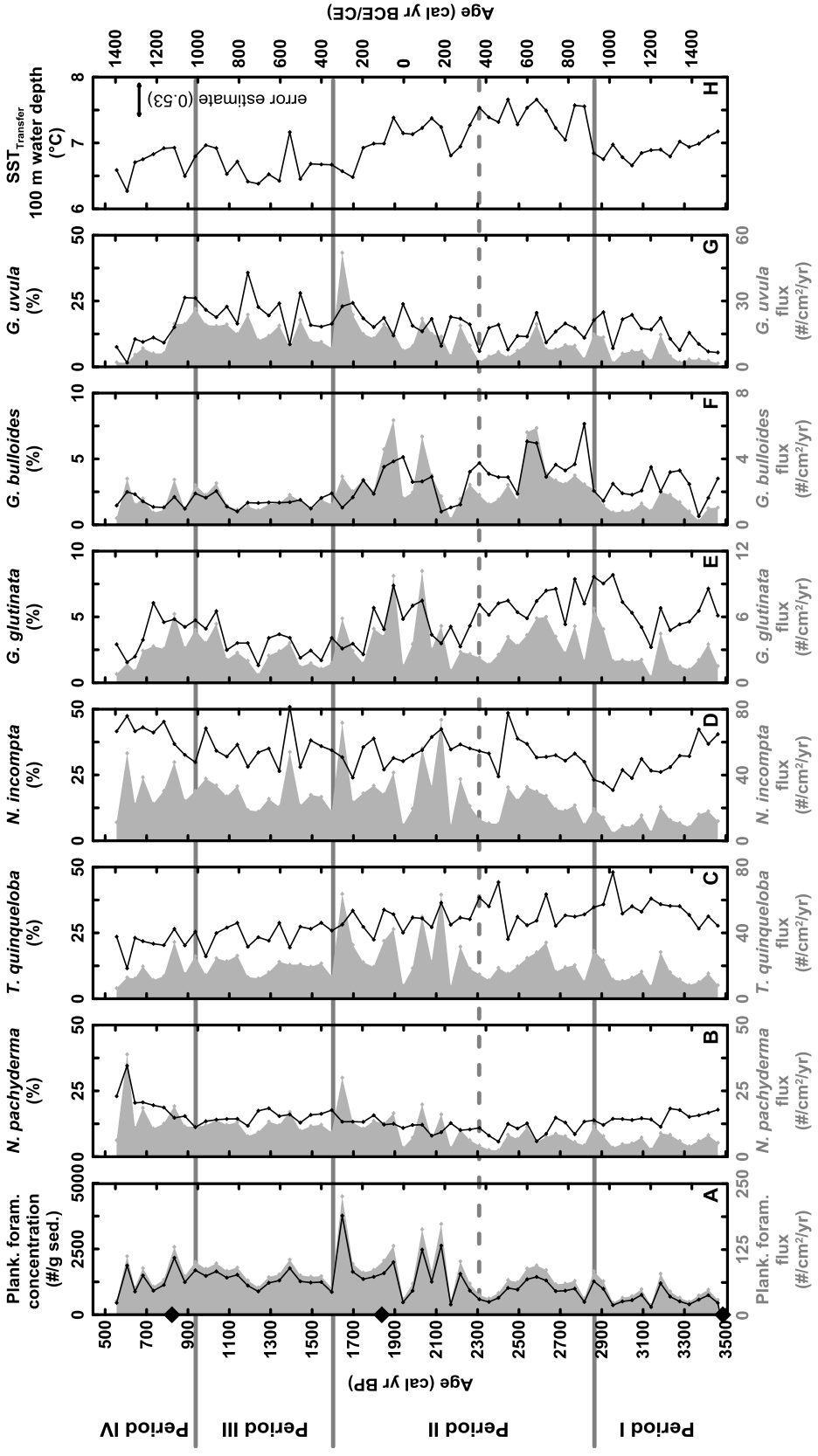
Age (cal yr BCE/CE)
1400 1200 1000 800 600 400 200 0 200 400 600 800 1000 1200 1400
SST Transfer 100 m water depth (°C)
error estimate (0.53)
H
G. uvula (%)
G. uvula flux (#/cm²/yr)
G
G. bulloides (%)
G. bulloides flux (#/cm²/yr)
F
G. glutinata (%)
G. glutinata flux (#/cm²/yr)
E
N. incompta (%)
N. incompta flux (#/cm²/yr)
D
T. quinqueloba (%)
T. quinqueloba flux (#/cm²/yr)
C
N. pachyderma (%)
N. pachyderma flux (#/cm²/yr)
B
Plank. foram. concentration (#/g sed.)
Plank. foram. flux (#/cm²/yr)
A
500 700 900 1100 1300 1500 1700 1900 2100 2300 2500 2700 2900 3100 3300 3500
Age (cal yr BP)
Period IV
Period III
Period II
Period I

Figure 5

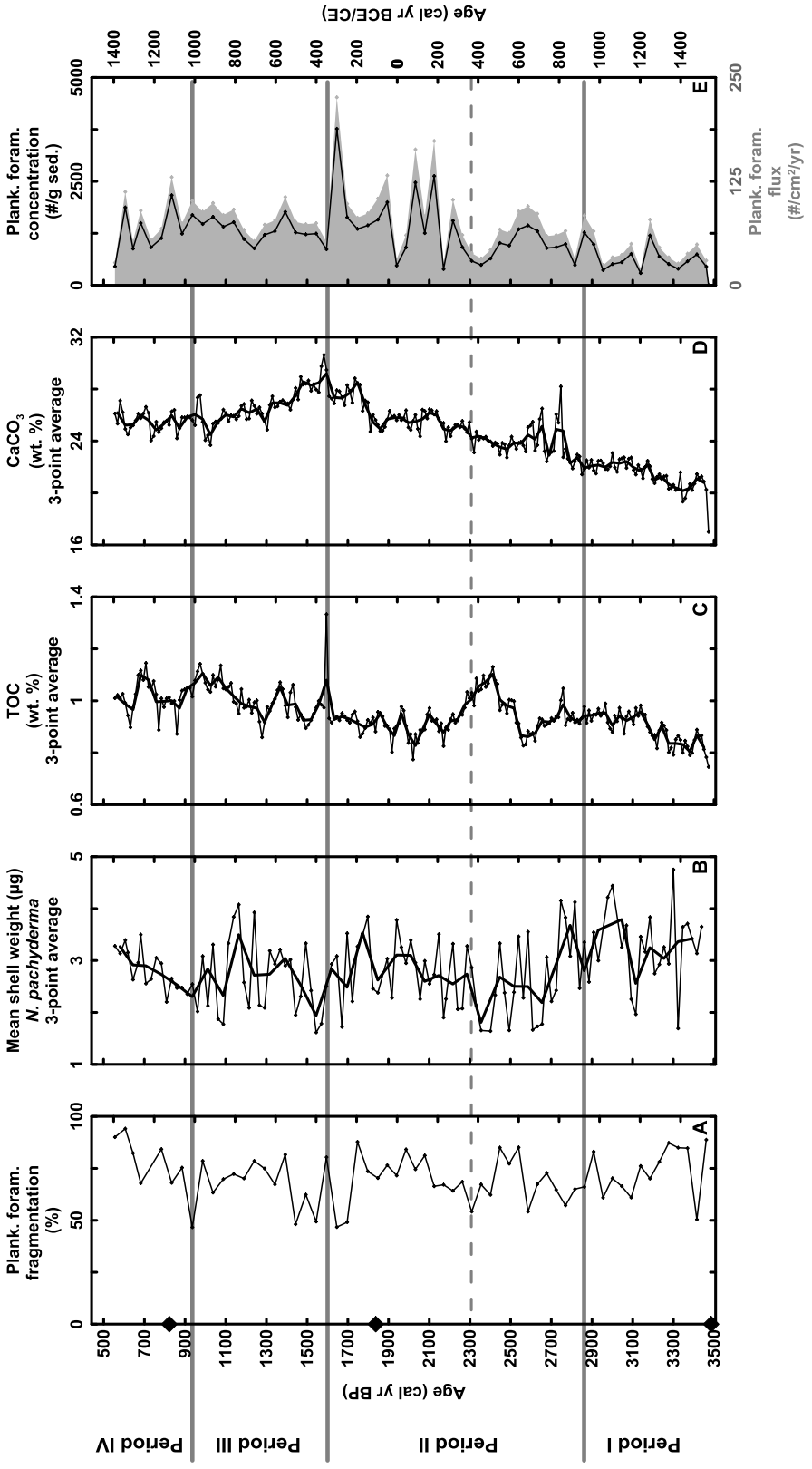
Age (cal yr BCE/CE)
1400 1200 1000 800 600 400 200 0 200 400 600 800 1000 1200 1400
Plank. foram. concentration (#/g sed.)
0 2500 5000
Plank. foram. flux (#/cm²/yr)
0 125 250
E
CaCO3 (wt. %) 3-point average
16 24 32
D
TOC (wt. %) 3-point average
0.6 1 1.4
C
Mean shell weight (µg) N. pachyderma 3-point average
1 3 5
B
Plank. foram. fragmentation (%)
0 50 100
A
Age (cal yr BP)
500 700 900 1100 1300 1500 1700 1900 2100 2300 2500 2700 2900 3100 3300 3500
Period IV
Period III
Period II
Period I

Figure 6

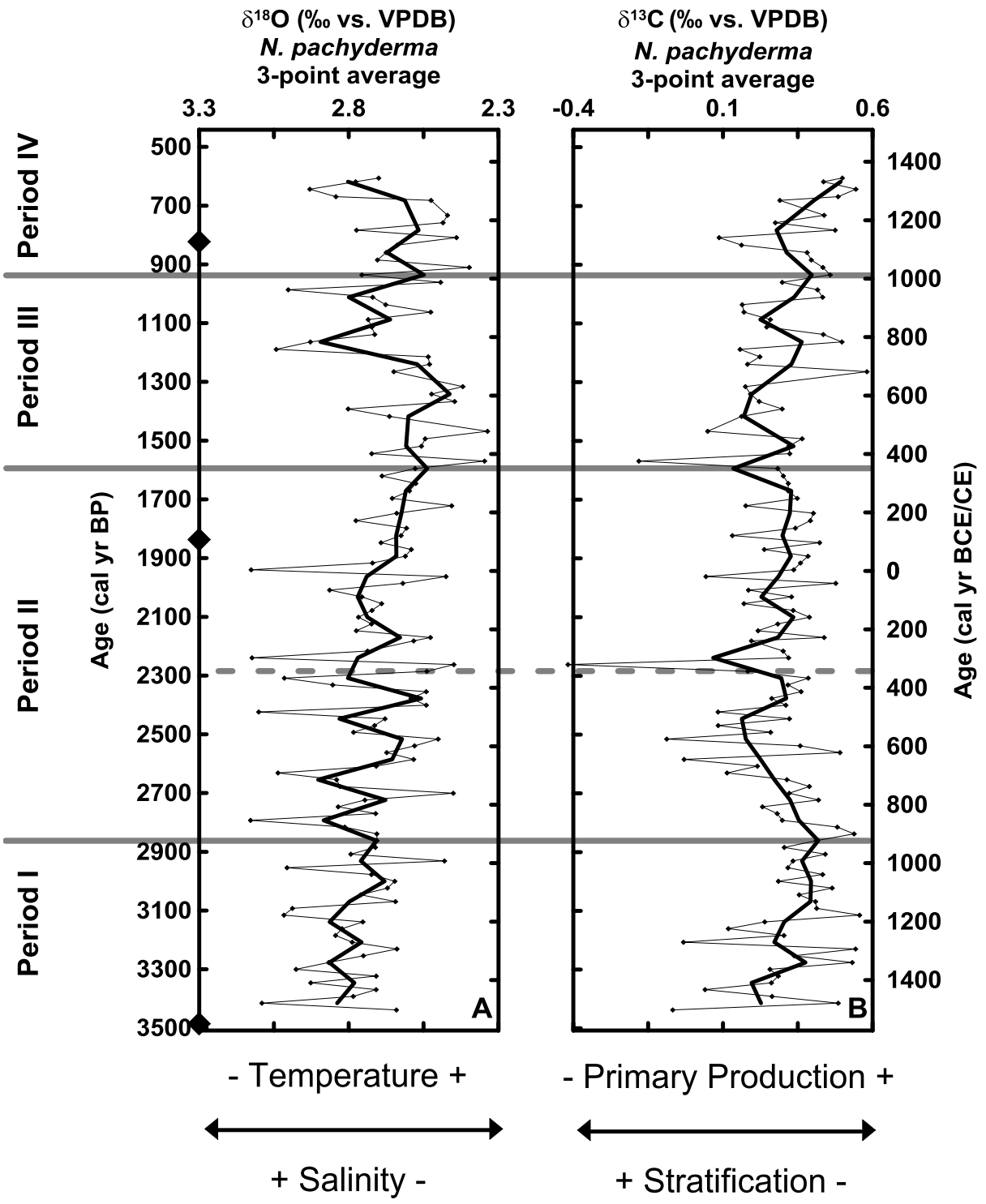
δ18O (‰ vs. VPDB)
N. pachyderma
3-point average
3.3
2.8
2.3
δ13C (‰ vs. VPDB)
N. pachyderma
3-point average
-0.4
0.1
0.6
Period IV
Period III
Period II
Period I
Age (cal yr BP)
500
700
900
1100
1300
1500
1700
1900
2100
2300
2500
2700
2900
3100
3300
3500
1400
1200
1000
800
600
400
200
0
200
400
600
800
1000
1200
1400
Age (cal yr BCE/CE)
A
B
- Temperature +
+ Salinity -
- Primary Production +
+ Stratification -

Figure 7

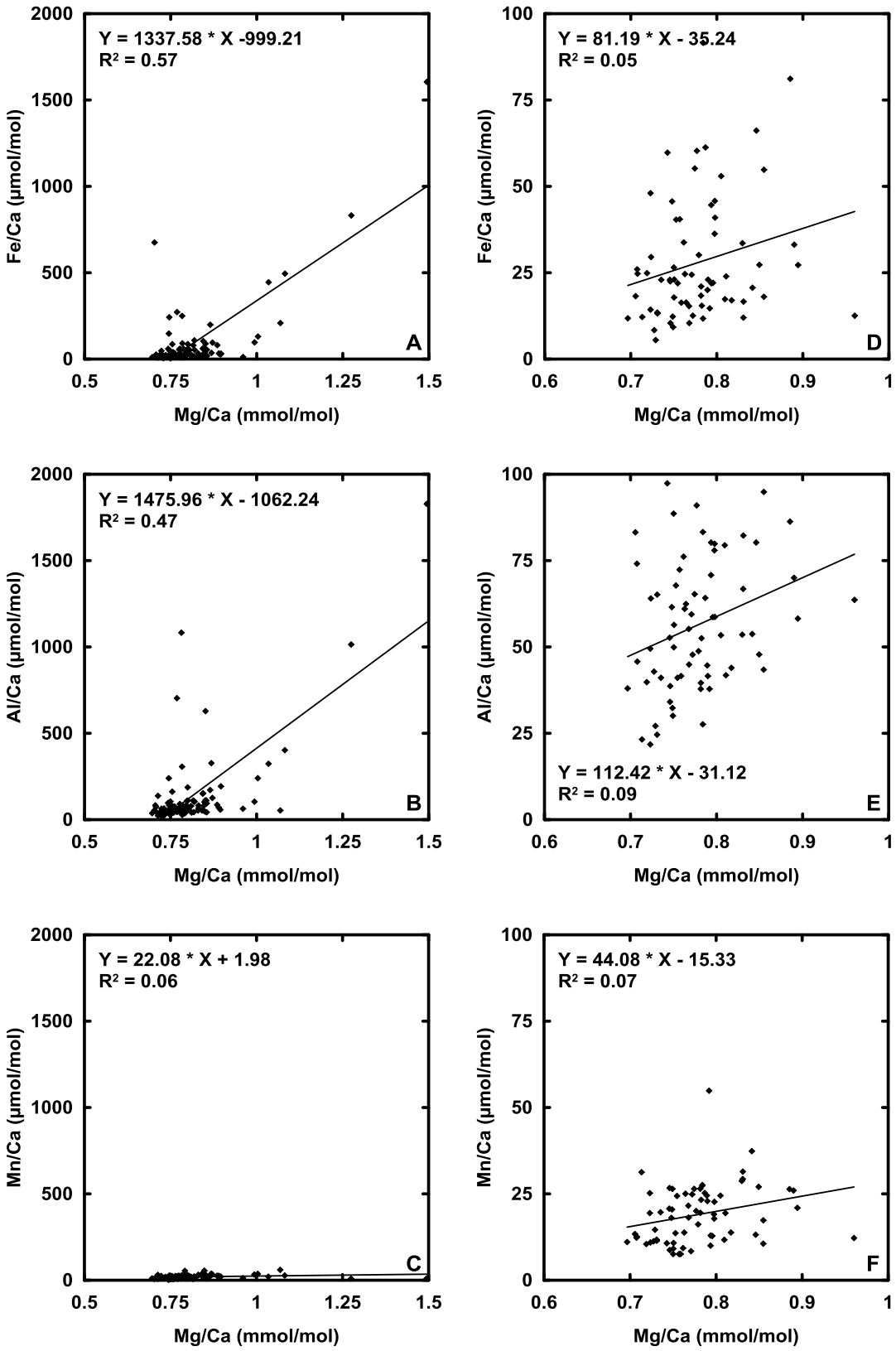
Y = 1337.58 * X -999.21
R² = 0.57
Fe/Ca (µmol/mol)
Mg/Ca (mmol/mol)
A
Y = 81.19 * X - 35.24
R² = 0.05
Fe/Ca (µmol/mol)
Mg/Ca (mmol/mol)
D
Y = 1475.96 * X - 1062.24
R² = 0.47
Al/Ca (µmol/mol)
Mg/Ca (mmol/mol)
B
Y = 112.42 * X - 31.12
R² = 0.09
Al/Ca (µmol/mol)
Mg/Ca (mmol/mol)
E
Y = 22.08 * X + 1.98
R² = 0.06
Mn/Ca (µmol/mol)
Mg/Ca (mmol/mol)
C
Y = 44.08 * X - 15.33
R² = 0.07
Mn/Ca (µmol/mol)
Mg/Ca (mmol/mol)
F

Figure 8

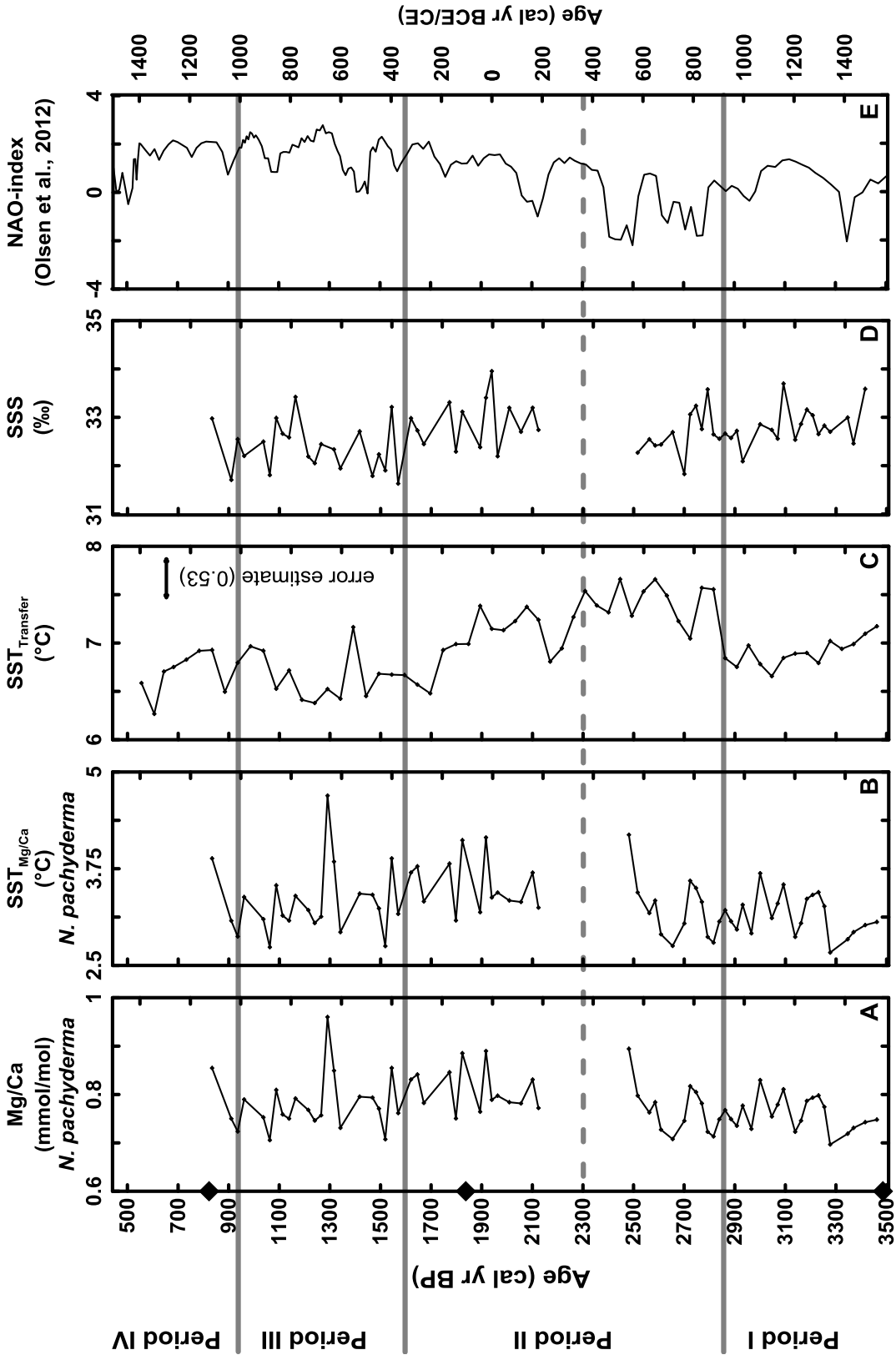
Age (cal yr BCE/CE)
1400
1200
1000
800
600
400
200
0
200
400
600
800
1000
1200
1400
NAO-index
(Olsen et al., 2012)
4
0
-4
E
SSS
(‰)
35
33
31
D
SST Transfer
(°C)
8
7
6
error estimate (0.53)
C
SST Mg/Ca
(°C)
N. pachyderma
5
3.75
2.5
B
Mg/Ca
(mmol/mol)
N. pachyderma
1
0.8
0.6
A
500
700
900
1100
1300
1500
1700
1900
2100
2300
2500
2700
2900
3100
3300
3500
Age (cal yr BP)
Period IV
Period III
Period II
Period I

Figure 9

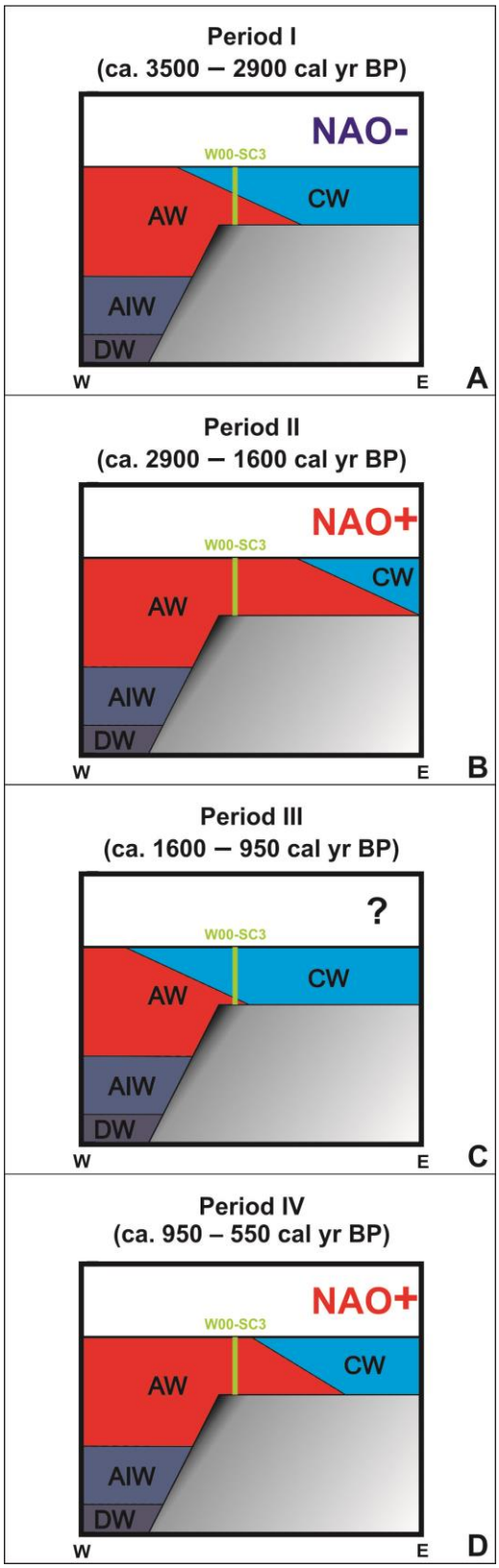
Period I
(ca. 3500 – 2900 cal yr BP)
NAO-
W00-SC3
AW
CW
AIW
DW
W
E
A
Period II
(ca. 2900 – 1600 cal yr BP)
NAO+
W00-SC3
AW
CW
AIW
DW
W
E
B
Period III
(ca. 1600 – 950 cal yr BP)
?
W00-SC3
AW
CW
AIW
DW
W
E
C
Period IV
(ca. 950 – 550 cal yr BP)
NAO+
W00-SC3
AW
CW
AIW
DW
W
E
D